https://doi.org/10.5194/egusphere-2025-3538
Preprint. Discussion started: 29 September 2025

Insights into the high temporal variability of atmospheric carbon dioxide (CO_2) at a suburban station in the Indo-Gangetic Plain

Vimal Jose Vazhathara[1,*], Ravi Kumar Kunchala[1], Sajeev Philip[1], Jaswant Rathore[1], Dilip Ganguly[1], Sagnik Dey[1,2], Yutaka Matsumi[3,4] and Prabir K. Patra[3,5]

[1]Centre for Atmospheric Sciences, Indian Institute of Technology Delhi, New Delhi, India.

[2]Centre of Excellence for Research on Clean Air, Indian Institute of Technology Delhi, New Delhi, India

[3]Research Institute for Humanity and Nature, Kyoto, Japan

[4]Institute for Space-Earth Environmental Research, Nagoya University, Nagoya, Japan

[5]Japan Agency for Marine-Earth Science and Technology (JAMSTEC), Yokohama, Japan.

*Correspondence to: Vimal Jose Vazhathara (vimaljosevazhathara@gmail.com), Centre for Atmospheric Sciences, Indian Institute of Technology Delhi, New Delhi, 110016, India

Abstract

The unusual weather patterns and large anthropogenic emissions over the Indo-Gangetic Plain (IGP) make it a significant hotspot of greenhouse gases like carbon dioxide (CO_2). Given the paramount significance of the IGP, a GHG observatory was set up at a suburban monitoring station, Sonipat, Haryana (28.95 °N, 77.10 °E), in the Delhi National Capital Region. Using continuous measurements of CO_2 using a laser-based cavity ring-down spectroscopy (CRDS) technique, we investigated the temporal evolution of CO_2 mole fraction from February 2023 to January 2025. We observed an annual average CO_2 mole fraction of 440.8 ± 19.7 parts per million (ppm) with an unusually strong seasonal variability ranging from 422.6 ± 23.3 to 456.4 ± 30.8 ppm in monsoon and post-monsoon, respectively. A strong CO_2 diurnal amplitude of 29 ppm in May and 63 ppm in October was observed mainly due to seasonal changes in boundary layer mixing and biospheric activity. Further investigation of the drivers of this unique feature (strong seasonal and diurnal CO_2 variability) over IGP revealed a strong contrast

https://doi.org/10.5194/egusphere-2025-3538
Preprint. Discussion started: 29 September 2025

to other global monitoring stations in the same latitude band. A strong correlation between CO_2 and CH_4 indicated a co-located emission source, while the strong positive correlation between CO_2 and carbon monoxide (CO) during post-monsoon indicates the footprint of crop residue burning on CO_2 mole fraction. We demonstrate that the high temporal CO_2 variability in the IGP is driven by the interplay of local anthropogenic and biomass burning emissions, biospheric fluxes, and prevailing meteorology.

1. Introduction

Carbon dioxide (CO_2) is the major greenhouse gas (GHG) contributing to climate change and global warming (IPCC, 2021; Fawzy et al., 2020). Due to the long lifetime and high radiative forcing potential, CO_2 can have a significant impact on global and regional climate (Wang et al., 2010). The atmospheric mole fraction of CO_2 has increased from 278 parts per million (ppm) in the pre-industrial period to 427 ppm in 2025 (NOAA, https://gml.noaa.gov). This rapid increase in the atmospheric fraction of CO_2 is primarily due to the combustion of fossil fuels, cement manufacture, deforestation, and other industrial processes (Stocker et al., 2013; Huang et al., 2016; Yoro and Daramola, 2020). A comprehensive understanding of the sources and sinks of CO_2 is critical for developing national policies to mitigate climate change impacts.

India is the third highest CO_2 emitting nation (8% of total global CO_2) in the last decade as reported by the Global Carbon Project (GCP) (Friedlingstein et al., 2025; Le Quéré et al., 2018). In particular, the Indo-Gangetic Plain (IGP) region is one of the hotspots for atmospheric CO_2 mole fraction primarily due to the large fossil fuel emissions and adverse meteorology (Kuttippurath et al., 2022; Singh et al., 2022). Over the past few decades, the IGP region has witnessed rapid urbanisation, industrialisation, and agricultural intensification, leading to significant changes in land-use patterns and GHG emissions (Yoro and Daramola, 2020). Mitigation of anthropogenic CO_2 emissions over the highly populated IGP region is crucial for reducing high atmospheric CO_2 mole fraction build-up. Gaining a better understanding of the magnitude of CO_2 sources and sinks and the local drivers of CO_2 temporal variability over the IGP region is therefore important.

The continuous monitoring of ground-based CO_2 is of utmost importance for the inverse modelling approaches to understand the sources and sinks of CO_2. Although GHG mole fraction have been monitored over various parts of the globe for decades, monitoring stations of GHGs in India are limited (Chakraborty et al., 2020; Kumar et al., 2021; Patra et al., 2013;

https://doi.org/10.5194/egusphere-2025-3538
Preprint. Discussion started: 29 September 2025

Tiwari et al., 2013) The Cape Rama (15.08° N, 73.83° E), situated on India's southwest coast, was the first Indian monitoring station tracking CO_2 mole fraction from 1993 to 2002 (Bhattacharya et al., 2009; Patra et al., 2011; Rayner et al., 2008). Recently, several monitoring stations have been established over different parts of India to measure the GHGs (Chandra et al., 2016; Jain et al., 2021; Mahesh et al., 2015; Metya et al., 2021; Nomura et al., 2021; Pathakoti et al., 2023; Sreenivas et al., 2016; Thilakan et al., 2023; Tiwari et al., 2014). Some aircraft-based (Niwa et al., 2012; Patra et al., 2011; Schuck et al., 2012; Zhang et al., 2007) and satellite-based (Das et al., 2023; Kunchala et al., 2022; Nalini et al., 2019; Philip et al., 2022; Xiong et al., 2009) studies have also been conducted in the past. The incorporation of the regional in situ and aircraft-based measurements along with satellite column CO_2 retrievals reduced uncertainties in top-down CO_2 flux estimations (Huang et al., 2008; Niwa et al., 2012; Zhang et al., 2014). These studies highlighted the importance of regional ground-based observations in constraining Indian carbon cycle dynamics. However, the IGP region still lacks continuous measurements to track temporal evolution of atmospheric CO_2 mole fraction except for one station in Mohali (Thilakan et al., 2023).

To comprehensively understand the temporal CO_2 variability along with its magnitude and the drivers of CO_2 in the IGP region, we have conducted atmospheric CO_2 mole fraction measurements at Sonipat, a suburban station in the IGP region upwind of Delhi. The continuous measurements from February 2023 to January 2025 were conducted using the laser-based cavity ring-down spectroscopy technique. Here, we investigate the novel characteristics of the seasonal and diurnal variability of atmospheric CO_2 mole fraction over the Sonipat monitoring station. We then identify the key drivers of the observed temporal CO_2 variability over the Sonipat station to gain insights into the carbon cycle dynamics of the entire IGP region.

2. Materials and methods

2.1 Monitoring station

The measurements in this study were carried out at the Indian Institute of Technology Delhi (IIT Delhi) Centre for Atmospheric Sciences (CAS) - Atmospheric Observatory situated at Sonipat campus (28.95° N, 77.10° E, 228 m amsl altitude). Sonipat is an upwind suburban region of Delhi situated in the north Indian state of Haryana and a part of the Delhi National Capital Region (NCR). The monitoring station is surrounded by agricultural fields, a National Highway, and academic institutions. Figure 1 shows the location map of the monitoring station. The climatic conditions over this site are similar to Delhi which has sweltering summers, damp or moist monsoons (June - September), and extreme winters. Similar to Delhi, this region also

https://doi.org/10.5194/egusphere-2025-3538
Preprint. Discussion started: 29 September 2025

has frequent haze and smog with low visibility during winter (December - February) and post-monsoon (October - November) seasons. During post-monsoon season, Sonipat station experiences large transport of pollutants from the North-West direction. In addition to the pollutant transport, several local emissions sources exist in the region, such as small industries, vehicular sources, and local biomass burning.

2.2 Local measurements

2.2.1 GHG measurements

This study utilised the PICARRO G2301 GHG analyzer to measure major atmospheric GHG mole fraction. The PICARRO analyzer employs the Cavity Ring-Down Spectroscopy (CRDS) technique at 0.5 Hz to measure CO_2 mole fraction. The CRDS technique utilises the ring-down time of light intensity within the cavity to determine the mole fraction of CO_2, a method fundamentally different that other measurement techniques such as other techniques such as Non-dispersive Infrared Spectroscopy (NDIR) and Fourier Transform Infrared Spectroscopy (FTIR). The long sample interaction path length (approximately 20 km) is a characteristic of CRDS, which enhances sensitivity compared to conventional techniques based on light-intensity absorption. The cavity pressure operates at a very low pressure of 140 Torr. This isolates a single spectral feature with a resolution of 0.0003 cm^{-1}, ensuring a linear relationship between peak height or area and mole fraction. The CRDS offers precise and highly sensitive measurements of gases in ambient air with a temporal resolution of 5 seconds. The technique has been well validated for the measurements of atmospheric CO, CO_2, and CH_4 mole fraction, globally and over some Indian monitoring stations (Chandra et al., 2016; Chen et al., 2013; Jain et al., 2021).

In this study, the cavity temperature was maintained at 45°C throughout the measurement period to ensure the necessary etalon mechanical stability of the measurement cavity. The sample air was taken from the top of the building and above the tree canopy (10 meters above the instrument housing) using an external vacuum pump and Teflon tube at ~400 SCCM flow rate.

To better interpret the temporal variability in the atmospheric CO_2 mole fraction, we calculated the background CO_2 mole fraction at Sonipat. The background mole fraction are typically calculated from measurements over pristine sites free of local emission sources. The Sonipat station, lying on the upwind side of Delhi, is a suburban station with relatively cleaner air when compared to the urban city centre. However, Sonipat cannot be considered a pristine site due to the impact of local emissions from nearby industries and national highways.

https://doi.org/10.5194/egusphere-2025-3538
Preprint. Discussion started: 29 September 2025

Typically, two techniques are used to calculate background CO_2 mole fraction at such monitoring stations. The fifth percentile method is based on the fifth percentile of the daily data to calculate the background mole fraction (Ammoura et al., 2014; Chandra et al., 2016; Jain et al., 2021). The adaptive diurnal minimum variation selection (ADVS) method considers the diurnal minimum value as the daily background value (Apadula et al., 2019; Yuan et al., 2018). In this study, the comparison between the fifth percentile and the ADVS methods showed similar CO_2 background values (see Fig. S1). Therefore, we adopted one of the methods (ADVS) here to report the background CO_2 mole fraction at Sonipat station. The excess CO_2 mole fraction were then estimated by subtracting the hourly averaged values of CO_2 from the background mole fraction.

The measurements of the atmospheric CH_4 mole fraction were also conducted with the PICARRO G2301 GHG analyser. The GHG analyser employs the CRDS at 0.5 Hz to measure CH_4 mole fraction. The mole fraction of CH_4 were determined using the ring-down time of light intensity, similar to CO_2 mole fraction. Calibration was performed following the guidelines of the National Oceanic and Atmospheric Administration Earth System Research Laboratories (NOAA-ESRL, 2020) and the Integrated Carbon Observation System (ICOS) protocol (Laurent, 2016), using NOAA standard calibration cylinders. Further details of the calibration process are provided in Supplementary Section S1.

2.2.2 Trace gas measurements

In addition to the measurements of CO_2 and CH_4, we also utilised the measurements of trace gases to establish the species interrelationships and to identify drivers of GHG sources. We used a compact air quality measurement instrument with gas sensors (CUPI-G) to collect continuous measurements of air pollutants, including fine particulate matter ($PM_{2.5}$), nitric oxide (NO), nitrogen dioxide (NO_2), and carbon monoxide (CO). The sensors used in CUPI-G are a palm-sized optical $PM_{2.5}$ sensor developed by Panasonic, the CO-B4 Carbon Monoxide Sensor, and the NO-B4 Nitric Oxide Sensor, respectively. The CUPI-G was deployed on the roof of the I-Techpark building at the Sonipat campus of IIT Delhi.

2.2.3 Local meteorology measurements

A Vaisala Ceilometer lidar CL61 was installed on the rooftop of the I-Techpark building at IIT Delhi's Sonipat campus at the same location as the GHG analyser is located. The CL61 system is designed to provide real-time measurements of cloud base height (CBH) for up to five layers, along with depolarisation measurements, under all weather conditions. To determine the

https://doi.org/10.5194/egusphere-2025-3538
Preprint. Discussion started: 29 September 2025

Planetary boundary layer height (PBLH) from the range-corrected attenuated backscatter data, the gradient method (Summa et al., 2013) and the Wavelet Covariance Transform (WCT) method (Baars et al., 2008) were employed. Further details on PBLH calculations can be found in (Rathore et al., 2025). An automatic weather station (AWS) by Geonica, installed on the I-Tech building rooftop, collected meteorological data at 5-minute intervals. The data, including ambient temperature, relative humidity (RH), atmospheric pressure, wind speed and direction, precipitation, and incoming solar radiation, was retrieved using Datagraph-W4K 2.1.3.0 software and exported in CSV format. All sensors were meticulously calibrated and regularly cleaned to ensure accuracy and reliability.

2.3 Auxiliary data

2.3.1 ObsPack Data

To compare the seasonality of atmospheric CO_2 of Sonipat with other non-Indian sites in the same latitudinal band, we used the obspack_co2_1_GLOBALVIEWplus_v10.1_2024-11-13 (Schuldt et al., 2024). This dataset is constructed using the Observation Package (ObsPack) framework (Masarie et al., 2014). This product includes 625 atmospheric carbon dioxide datasets from observations made by 79 laboratories from 28 countries. The ObsPack dataset provides data for the period 1957-2023. We used the five-year averaged data for all sites except one (Boulder Atmospheric Observatory, Colorado) for 2018-2022 to further compare the seasonality over different locations across the globe.

2.3.2 Satellite CO_2 retrievals

Along with the ground-based in situ CO_2 measurements at the Sonipat monitoring station, we also used column average dry air CO_2 mole fraction (XCO_2) retrievals from the Orbiting Carbon Observatory-2 and 3 satellites (OCO-2 and OCO-3). The OCO-2 satellite provides data at a temporal frequency of 16 days with a spatial resolution of 1.29 km × 2.25 km (for nadir observations) (Crisp et al., 2017; Eldering et al., 2017). We used the bias-corrected OCO-2 v11.1r data product for the period from February 2023 to December 2024. The OCO-3 satellite provides XCO_2 data at a temporal frequency of 16 days with a spatial resolution of 1.60 km × 2.25 km (nadir observation) which increases the swath area from ~3.0 km^2 to ~3.5 km^2. We used bias-corrected OCO-3 v10.4r data product (Eldering et al., 2019; Srivastava et al., 2020) for February 2023 to December 2024.

2.3.3 FluxSat GPP

https://doi.org/10.5194/egusphere-2025-3538
Preprint. Discussion started: 29 September 2025

To study the Gross Primary Production (GPP) fluxes over Sonipat, we used FluxSat v2.2 native GPP product computed at the spatio-temporal resolution of the MCD43C data set (daily at 0.05° spatial resolution (Schaaf et al., 2002; Wang et al., 2018). FluxSat v2.2 has been derived from the MODerate resolution Imaging Spectroradiometer (MODIS) instruments on the NASA Terra and Aqua satellites using the collection 6.1 MCD43C Bidirectional Reflectance Distribution Function (BRDF)-Adjusted Reflectances (NBAR) (Joiner et al., 2018; Joiner and Yoshida, 2020; Schaaf and Wang, 2021). FluxSat v2.2 is "calibrated" using a set of the FLUXNET 2015 and OneFlux tier 1 (publicly released) eddy covariance (EC) data and has been compared with independent data (i.e., not used in the calibration) as validation. We used Global Gross Primary Production (GPP) estimates for 2023 in this study.

2.3.4 Ecosystem-proxy variables

We used two key ecosystem-proxy variables to study the carbon cycle dynamics of the Sonipat station and the IGP region. The Normalised Difference Vegetation Index (NDVI) version 5 data from the Advanced Very High-Resolution Radiometer (AVHRR) was used here (Vermote and NOAA CDR Program, 2018). This dataset consists of daily NDVI values retrieved from the National Oceanic and Atmospheric Administration's (NOAA) Climate Data Record (CDR) of AVHRR Surface Reflectance. The NDVI CDR summarises the surface vegetation coverage activity based on measurements in the red and near-infrared spectral bands. The NDVI CDR provides daily output on a global grid with a resolution of 0.05 degrees latitude by 0.05 degrees longitude from 1981 to the present.

To understand the photosynthetic capacity of the regional ecosystem to assimilate atmospheric CO_2, we used the Solar Induced chlorophyll Fluorescence (SIF) retrievals from the OCO-2 satellite (Frankenberg et al., 2014). The OCO-2 provides SIF data at a temporal resolution of 16 days and a spatial resolution of 1.35 km × 2.25 km. The estimation of SIF relies on evaluating the in-filling of solar Fraunhofer lines at 757 nm and 770.1 nm surrounding the O_2 A-band (Frankenberg et al., 2014; Sun et al., 2018). We used bias-corrected SIF data from OCO-2 v11r and v11.2r SIF data products for February 2023 to December 2024.

2.4 Models

2.4.1 JAMSTEC's MIROC version 4 atmospheric chemistry-transport model (MIROC4-ACTM)

We used the Model for Interdisciplinary Research on Climate version 4 (MIROC4;Watanabe et al., 2008), an atmospheric general circulation model (AGCM)-based chemistry-transport

https://doi.org/10.5194/egusphere-2025-3538
Preprint. Discussion started: 29 September 2025

model (MIROC4-ACTM; Patra et al., 2018), to simulate CO_2 mole fraction for this study. Simulations of long-lived gases (CO_2, CH_4, N_2O, SF_6) were performed at a horizontal resolution of T42 spectral truncations (~2.8° latitude–longitude grid) with 67 vertical hybrid-pressure layers between the Earth's surface and 0.0128 hPa (~80 km) (Bisht et al., 2021; Chandra et al., 2021; Patra et al., 2017, 2018). CO_2 tracers were simulated corresponding to the fossil fuel combustion ($FFCO_2$), land biosphere fluxes ($LBCO_2$), fire emissions (CO_{2fire}), and ocean exchanges (CO_{2ocn}) from different sets of prior (bottom-up) emissions (Chandra et al., 2022). $FFCO_2$ was simulated using the gridded fossil fuel emission dataset (GridFED; Jones et al., 2021). $LBCO_2$ tracers were simulated using two sets of terrestrial biosphere fluxes from the Carnegie-Ames-Stanford Approach (CASA) biogeochemical model (Randerson et al., 1997) and Vegetation Integrative Simulator for Trace Gases (VISIT) (Ito, 2019). For this study, we use simulated total CO_2 mole fraction and tracers.

2.4.2 CarbonTracker (CT) inverse model

To understand the temporal pattern of atmospheric CO_2 mole fraction over the study station and the IGP region, we used simulated CO_2 mole fraction from an inverse modelling framework CarbonTracker (CT) (Peters et al., 2005). Here, we used the CarbonTracker 2022 release (CT2022) which incorporated two-way nesting of the offline atmospheric tracer transport model TM5 supporting coarse-resolution data globally and high-resolution data regionally (Krol et al., 2004). The TM5 model in CT2022 was driven with meteorology from the ERA-interim reanalysis provided by the European Center for Medium-Range Weather Forecasts (ECMRWF) {Citation}. The CT2022 inverse model simulated atmospheric CO_2 mole fraction by correcting the prior specifications of CO_2 sources and sinks in the model by assimilating global in situ observations. In this study, we used CT2022-simulated CO_2 mole fraction from February 2023 to October 2023.

2.4.3 GEOS-Chem inverse model

To study the seasonality of the fluxes over Sonipat, we used a four-dimensional variational (4D-Var) assimilation system with the GEOS-Chem global chemical transport model (CTM;Philip et al., 2019, 2022). The GEOS-Chem 4D-Var system was constrained with XCO_2 retrievals from the OCO-2 satellite (Philip et al., 2022), following the protocol of the OCO-2 v10 Multi-model Intercomparison Project (MIP) (Byrne et al., 2017; Liu et al., 2014). The Net

https://doi.org/10.5194/egusphere-2025-3538
Preprint. Discussion started: 29 September 2025

Ecosystem Exchange (NEE) fluxes for 2023 at a spatial resolution of 1° × 1°, constrained with the OCO-2 Land Nadir and Land Glint observational modes are used here.

2.4.4 Mi CASA terrestrial biospheric model

We simulated CO_2 fluxes from a terrestrial biospheric model (TBM) have also been used in this study. The Más informada Carnegie-Ames-Stanford-Approach (Mi CASA) model (Weir, 2024), a comprehensive update to the CASA – Global Fire Emissions Database, version 3 (CASA-GFED3) product, was utilised here (Chen et al., 2023; Potter et al., 1993). Mi CASA provides daily global data at 0.1° resolution from January 2001 to December 2023. This includes carbon flux variables from sources such as net primary production (NPP), heterotrophic respiration (Rh), wildfire emissions (FIRE), and fuel wood burning emissions (FUEL). The model is driven with meteorological data from NASA's Modern-Era Retrospective analysis for Research and Application, Version 2 (MERRA-2). Previous studies used the MERRA-driven CASA GFED to investigate the carbon cycle dynamics (Campbell et al., 2008; Hammerling et al., 2012; Kawa et al., 2010; Ott et al., 2015; Weir et al., 2021a, b). We used Mi CASA model simulated NEE, NPP, and Rh fluxes over the Sonipat station for this study.

https://doi.org/10.5194/egusphere-2025-3538
Preprint. Discussion started: 29 September 2025

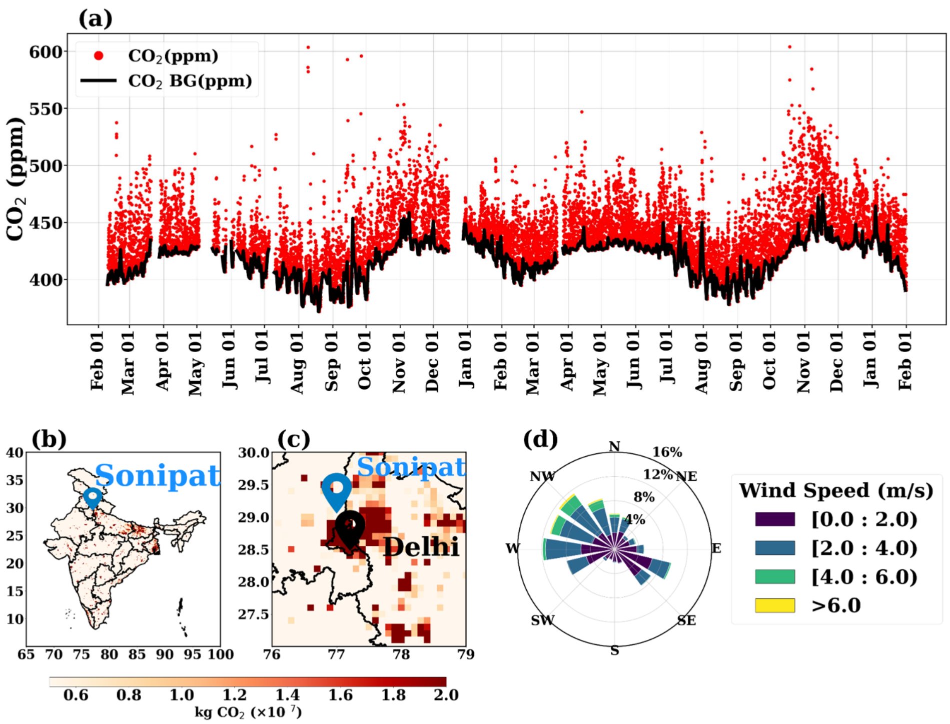

Figure 1: (a) Hourly averaged time series of atmospheric CO_2 (red) mole fraction for the study period (February 2023 to January 2025) over Sonipat. The thick black line represents the background mole fraction estimated using the Adaptive Diurnal least Variation Selection (ADVS). Anthropogenic CO_2 emissions over (b) India and (c) Sonipat/Delhi are derived from the EDGAR emission inventory for 2021. (d) Annually averaged wind patterns over Sonipat for February 2023 – January 2024.

3. Results and discussions

3.1 CO_2 measurements at Sonipat station

Figure 1(a) shows hourly averaged time series of atmospheric CO_2 mole fraction at the Sonipat station from February 2023 to January 2025. During this period, hourly CO_2 varies in the range from ~380 ppm to ~ 550 ppm, with the highest values observed in November 2024 indicating the large variability in the regional CO_2 build-up at the study location. The strong seasonal and diurnal variations are evident during the entire study period. In general, minimum variability and lowest mole fraction of CO_2 are found from July to August, while strong variability and

https://doi.org/10.5194/egusphere-2025-3538
Preprint. Discussion started: 29 September 2025

high mole fraction are visible from October to November. We found annual mean CO_2 mole fraction of 440.8 ± 19.7 ppm during the study period. Table S1 compares the annual mean CO_2 mole fraction values with other measurement network stations in India. Interestingly, the annual mean values for different stations in India, even rural sites like Gadanki and urban sites like Ahmedabad, have consistent values.

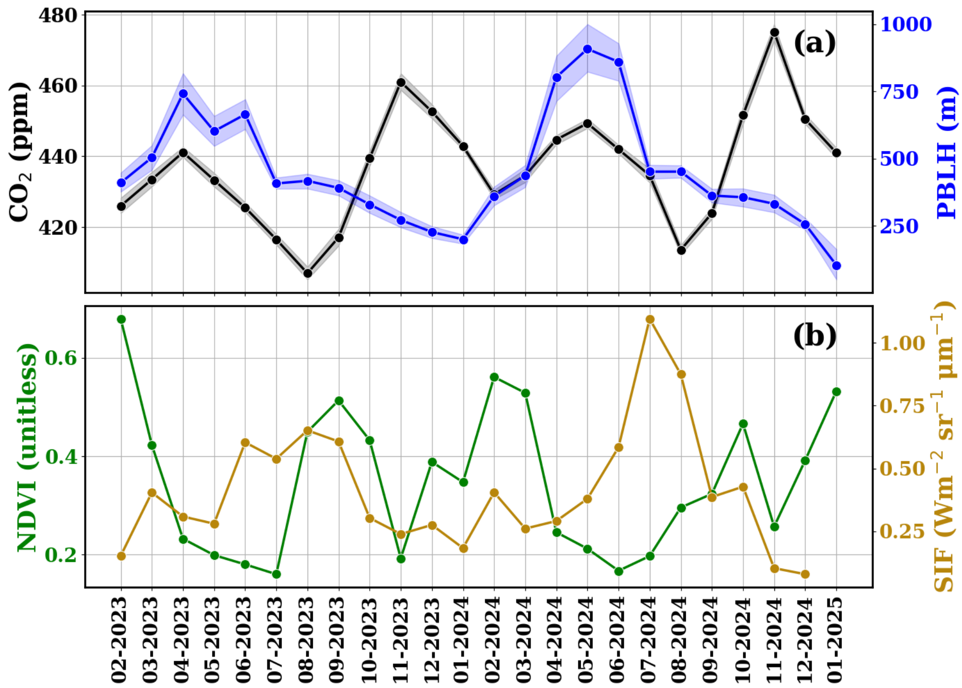

Figure 2: (a) Monthly variations of atmospheric CO_2 mole fraction (black) and PBLH (blue) and (b) NDVI (green) and SIF (olive green) over the Sonipat monitoring station during the study period.

Figures 1(b) and 1(c) illustrate the annual mean anthropogenic CO_2 emissions over India and Sonipat for 2021 based on the EDGAR emission inventory, and it is observed that the Delhi NCR is a hotspot of anthropogenic CO_2 emissions. Figure 1(d) shows that the dominant wind direction over Sonipat during the study period was from the northwest, indicating significant influence from upwind sources of pollution and greenhouse gases. To better understand the local meteorology, we analysed the seasonal variations of various meteorological parameters such as air temperature, wind speed, wind direction and relative humidity (Fig. S2). Figure S3 presents the seasonally averaged wind rose diagrams over

https://doi.org/10.5194/egusphere-2025-3538
Preprint. Discussion started: 29 September 2025

Sonipat. It is evident that the predominant wind pattern is from the northwest. In this study, we focus on seasonal and diurnal CO_2 variability and compare these patterns with other stations in India and the same latitudinal band across the globe to uncover the unique aspects of CO_2 dynamics over Sonipat and the IGP as well.

3.2 Seasonal variability

3.2.1 Seasonality of in situ observations

Figure 2 shows the monthly mean atmospheric CO_2 mole fraction during the study period. The shaded region represents a 95 percent confidence interval of the monthly mean CO_2 mole fraction. The monthly mean mole fraction of CO_2 shows a maximum in November (post-monsoon season) and a minimum in August (monsoon season) during both years. The average seasonal mean values of CO_2 observed during different seasons are 440.8 ± 19.7 ppm (pre-monsoon), 422.6 ± 23.3 ppm (monsoon), 456.4 ± 30.8 ppm (post-monsoon), and 440.5 ± 19.7 ppm (winter).

The seasonal cycle of CO_2 is mostly governed by the strength of emission sources, photosynthetic activity (biospheric fluxes), local meteorology and atmospheric transport. One of the key factors that controls the local variability of atmospheric CO_2 is planetary boundary layer height (PBLH). This is the lowest layer within the troposphere, where temperature and wind speed variations are integral in modulating its height. Strong vertical mixing in a well-developed boundary layer can dilute GHG mole fraction near the surface. Therefore, the seasonal changes in the PBLH affect the atmospheric CO_2 mole fraction near the surface. Figure 2(a) shows that the minimum values in PBLH during pre-monsoon months and maximum values during winter. During pre-monsoon, deep convection due to the well-developed PBLH from the surface to the upper troposphere results in lower mole fraction as compared to the winter months (Baker et al., 2012; Kar et al., 2004; Park et al., 2009; Patra et al., 2011; Randel and Park, 2006).

To better understand the seasonal patterns of CO_2 mole fraction, we examined its relationship with the normalised difference vegetation index (NDVI) and solar-induced fluorescence (SIF). Both NDVI and SIF are widely used indicators of vegetation cover and photosynthetic activity (Aburas et al., 2015; Nath, 2014). Our analysis shows a strong inverse relationship between CO_2 levels and NDVI, as illustrated in Fig. 2. Figure 2(b) reveals that vegetation growth starts with the onset of the monsoon season. An enhanced vegetation cover

https://doi.org/10.5194/egusphere-2025-3538
Preprint. Discussion started: 29 September 2025

over the region from August and a noticeable decrease in atmospheric CO_2 mole fraction is evident. Increased vegetation cover shows an increase in the photosynthetic carbon uptake by the biosphere, which decreases atmospheric CO_2 mole fraction. However, as vegetation activity declines from the post-monsoon to winter and pre-monsoon seasons, photosynthetic carbon uptake decreases, leading to a rise in atmospheric CO_2. The negative correlation of NDVI versus CO_2 mole fraction was found for most locations in India (Metya et al., 2021; Sreenivas et al., 2016; Tiwari et al., 2014), indicating the strong dependence of CO_2 seasonality on the local vegetative carbon uptake.

A sharp decrease in seasonal mean (~ 18 ppm) is visible from pre-monsoon to monsoon. This is attributed to the enhanced photosynthetic activity around the measurement site due to the availability of large soil moisture. A further decrease in CO_2 mole fraction is also observed as the monsoon progresses, with minimum mole fraction observed in August. The decreases in temperature (due to cloudy and overcast conditions prevailing during these months) reduce leaf and soil respiration, which contributes to the enhancement of carbon uptake (Jing et al., 2010; Patil et al., 2014). Further, an increase in CO_2 mole fraction (~ 34 ppm) is observed during post-monsoon, which is associated with higher ecosystem productivity (Sharma et al., 2014) and an enhancement in soil microbial activity (Kirschke et al., 2013). The gradual decrease in NDVI during this period indicates a decrease in CO_2 uptake by vegetation. This season coincides with crop-burning episodes in northern India. The crop-burning residue activities significantly contribute to the increase in CO_2 mole fraction. A sharp decrease (~ 16 ppm) in seasonal mean during the winter is evident compared to post-monsoon. The shallow PBLH and winds from western IGP that transport crop-burning residue contribute to the enhanced mole fraction during winter. Table S2 compares the seasonal amplitude and the peak and draw-down months over the measurement site with similar studies over India. Sonipat exhibits higher seasonal amplitudes than other sites. However, a similar pattern in CO_2 peak and drawdown months is evident in other monitoring stations.

3.2.2 Constraints from model and satellites

Figure 3 shows the comparison of ground-based mole fraction of CO_2 with the CarbonTracker inverse model (CT2022) simulated mole fraction (see different y-axis). The model outputs beyond October 2023 were not publicly available. In general, the CT2022 model-simulated mole fraction are much lower than observed mole fraction at the Sonipat station. The discrepancy could be mainly due to the representativeness issue, due to the coarser model

https://doi.org/10.5194/egusphere-2025-3538
Preprint. Discussion started: 29 September 2025

spatial resolution. Nevertheless, the seasonal pattern of CO_2 mole fraction simulated with the model is in broad agreement with observations (Fig. 3). The CT2022 model simulates the seasonal variability with a minimum mole fraction of 416 ppm during September, whereas in situ measurements show a minimum mole fraction of 407 ppm during August. The CT2022 model exhibits higher mole fraction during the pre-monsoon season, similar to in situ data. Note that most global and regional chemical transport models were unable to reproduce the large seasonal magnitude of surface-based measured atmospheric CO_2 mole fraction for any of the monitoring stations in India with different land ecosystems (Lin et al., 2018; Philip et al., 2022).

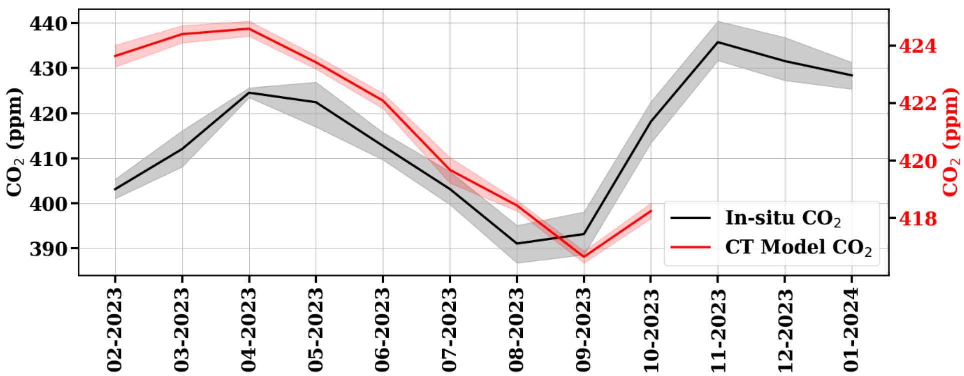

Figure 3: Monthly mean background CO_2 mole fraction over Sonipat (estimated using ADVS method) compared to CarbonTracker (CT2022) model simulated values at daytime (13:00 – 16:00). Note that the left y-axis represents surface mole fraction from in situ measurements, and the right y-axis represents CT2022-simulated mole fraction.

https://doi.org/10.5194/egusphere-2025-3538
Preprint. Discussion started: 29 September 2025

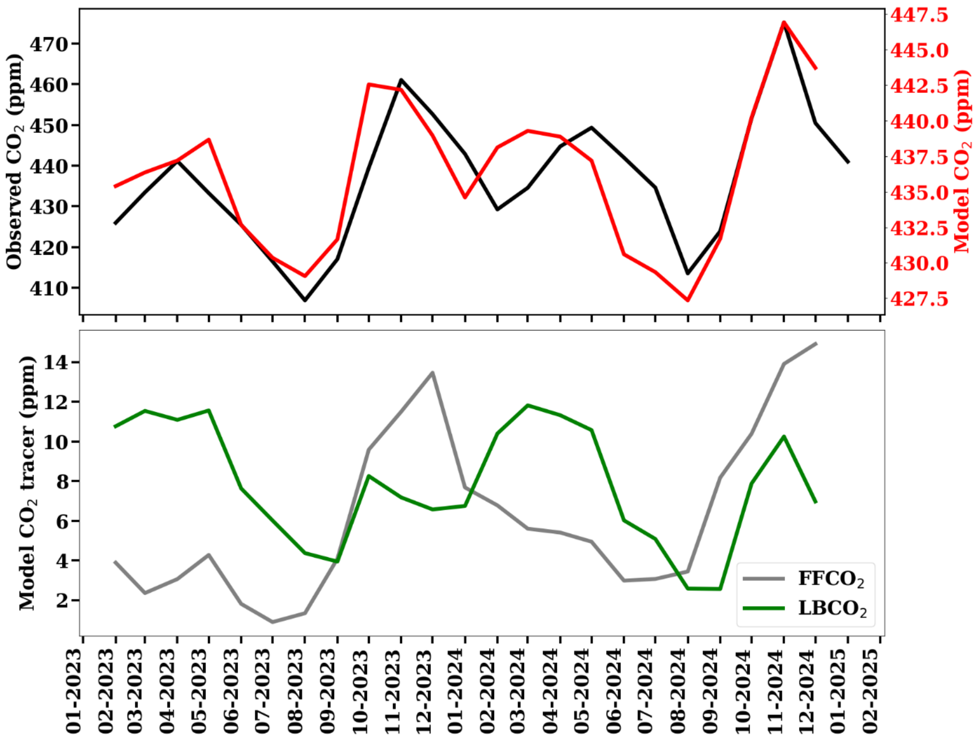

Figure 4: (a) Comparison of simulated mole fraction of atmospheric CO_2 from MIROC-ACTM with in situ measurements at Sonipat and (b) monthly averaged time series of different tracers from the MIROC-ACTM.

Figure 4(a) presents the comparison of atmospheric mole fraction of CO_2 over Sonipat with simulated mole fraction of CO_2 from the MIROC4-ACTM model. The model has well captured the seasonal pattern of CO_2, but it fails to capture the seasonal amplitude over Sonipat. The highs during post-monsoon and the drawdown during pre-monsoon show a strong correlation with in situ measurements. Figure 4(b) presents the monthly averaged time series of model-simulated CO_2 tracers. The fossil fuel tracer ($FFCO_2$) exhibits a peak in post-monsoon with a gradual decrease in winter and a drawdown in monsoon, which coincides with observed CO_2 mole fraction. The post-monsoon peak can be attributed to the added emissions from crop residue burning, which is a characteristic of the site. The drawdown in monsoon can be attributed to the added soil moisture and increased CO_2 uptake by plants during this time (further discussed in section 3.4). $LBCO_2$ presents a peak during pre-monsoon and a drawdown in monsoon. The peak can be attributed to dry soil conditions and a lack of vegetation during

https://doi.org/10.5194/egusphere-2025-3538
Preprint. Discussion started: 29 September 2025

this time. A similar enhancement of $LBCO_2$ is visible during the post-monsoon season, which coincides with the harvest period over the site. The lack of vegetation with added CO_2 from crop residue burning contributes to this enhancement. The drawdown in mole fraction during the monsoon season is due to wetter soil conditions and enhanced biospheric activity.

Figure 5 compares XCO_2 from OCO-2 and OCO-3 satellites with ground-based CO_2 measurements at Sonipat during the study period. The XCO_2 reveals a similar seasonal pattern with high mole fraction during the pre-monsoon season, followed by a dip in mole fraction during the monsoon season and a further gradual increase in mole fraction during the post-monsoon and winter months. Although the satellite column data captures the monthly variability reasonably well, it fails to capture the sharp increase in mole fraction during the post-monsoon. This enhancement during the post-monsoon season can be attributed to crop residue burning over the monitoring station and the added transport from Punjab (see Section 3.5). This highlights the inability of high-resolution satellite data to capture enhancements from local sources.

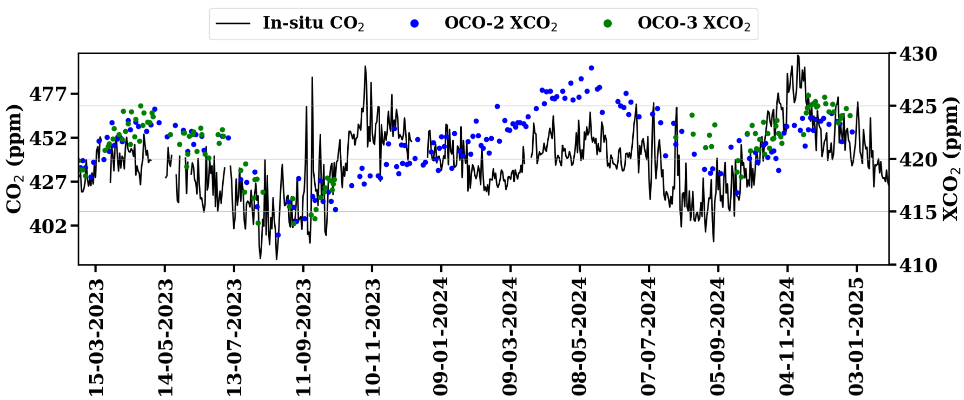

Figure 5: Daily variations of atmospheric CO_2 mole fraction from in situ measurements over Sonipat (left y-axis) with column average CO_2 mole fraction (XCO_2) from the OCO-2 (ppm) and OCO-3 (ppm) satellite instruments (right y-axis).

3.2.3 Comparison with data from other monitoring stations

https://doi.org/10.5194/egusphere-2025-3538
Preprint. Discussion started: 29 September 2025

Figure 6(a) presents the monthly averaged variation of CO_2 over Sonipat during the study period (SNT) with other measurement sites in the same latitudinal band (5° N – 40° N). The other sites used for comparison include five Indian monitoring stations and six international stations. The five Indian sites that reported CO_2 mole fraction were Shadnagar (SDN; 17.09° N, 78.2° E), Gadanki (GDN; 13.50° N, 79.20° E), Mohali (MHL; 30.67° N, 76.73° E), Sinhagad (SNG; 18.21° N, 73.45° E) and Ahmedabad (AHM; 23.03° N, 72.55° E). Apart from Indian sites, six sites in the same latitudinal band (using ObsPACK) were compared. These sites were Mauna Lou (MLO; 19.54° N, 155.58° W), South Carolina (SCT; 33.40° N, 81.83° W), Shenandoah National Park (SNP; 38.61° N, 78.35° W), Walnut Grove, (WGC; 38.26° N, 121.49° W), Moody (WKT; 31.31° N, 97.33° W) and Boulder (BAO; 40.05° N, 105.00° W). Figure 6b compares the seasonal amplitude of the sites in the chosen latitudinal band. The inset in Fig. 6b shows the location of all the measurement sites. For all non-Indian sites except BAO, the five-year average (2018-2022) has been chosen for the seasonality. For BAO, 2011-2016 has been used for this study.

https://doi.org/10.5194/egusphere-2025-3538
Preprint. Discussion started: 29 September 2025

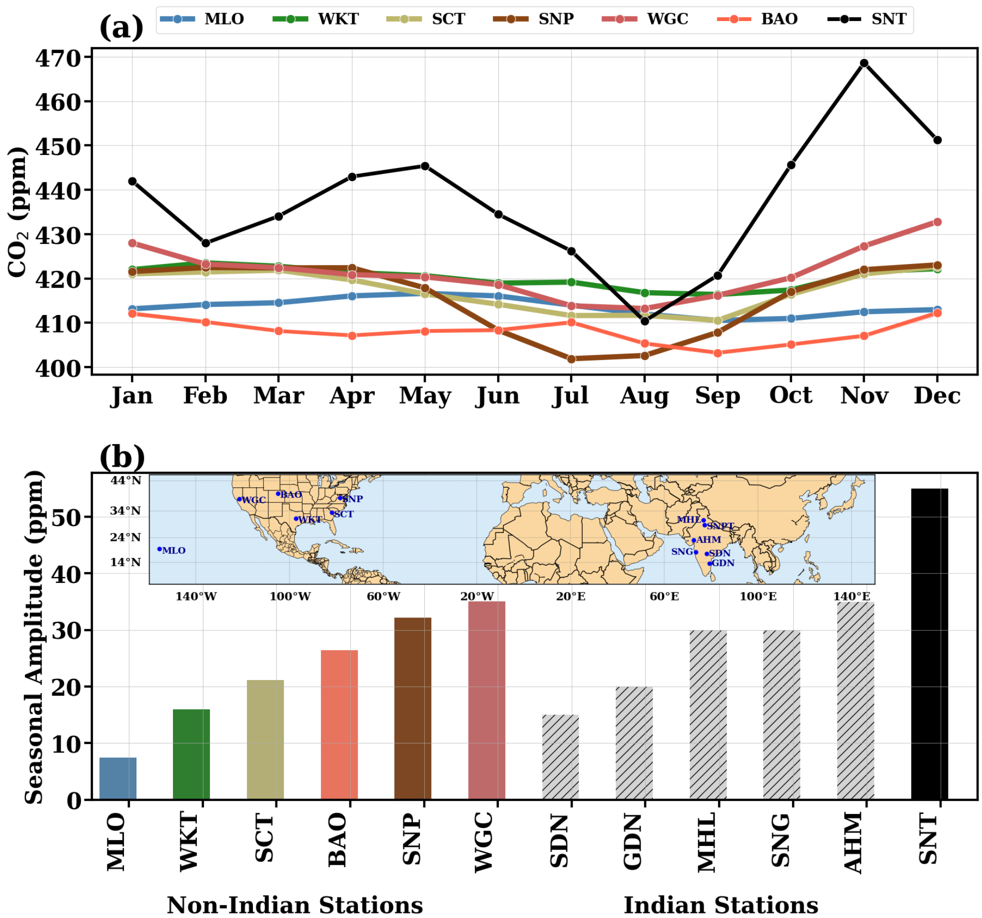

Figure 6: (a) Comparison of the seasonal variability of atmospheric CO_2 over Sonipat monitoring station with various locations in the same latitudinal band. (b) Comparison of the seasonal amplitude between Indian (coloured bars) and international monitoring stations (grey bars). Indian stations include Shadnagar (SDN), Sinhagad (SNG), Ahmedabad (AHM), Mohali (MHL), Gadanki (GDN), and Sonipat (SNT). International stations include Mauna Loa (MLO), South Carolina (SCT), Shenandoah National Park (SNP), Walnut Grove, (WGC), Moody (WKT) and Boulder (BAO). For all international stations except BAO, the five-year average (2018 - 2022) has been chosen for the seasonality. For BAO, 2011 – 2016 has been used. The monthly average of the entire study period (February 2023 – January 2025) has been used for this comparison.

Sonipat exhibits very high seasonal amplitude (~ 60 ppm) compared to other sites (~ 15 ppm) across the globe, however, the seasonal amplitude is around 35 ppm at Ahmedabad.

https://doi.org/10.5194/egusphere-2025-3538
Preprint. Discussion started: 29 September 2025

The major attribution to the high seasonal amplitude of CO_2 at Sonipat occurs during post-monsoon (Fig. 6a). This high amplitude for November has been observed during 2023 and 2024 (see Fig. 2), a characteristic of the Sonipat station. The high seasonal amplitude is associated with the crop residue burning season over Haryana and Punjab (further discussed in section 3.5). Being surrounded by agricultural land, Sonipat is prone to emissions from crop residue burning. The location of the measurement site in IGP on the downwind of Punjab is a major reason for this strong seasonal variability compared to other sites in the same latitudinal band.

3.3 Diurnal variability

Figure 7 (a-d) presents the averaged diurnal variation of atmospheric CO_2 mole fraction and PBLH at Sonipat during four seasons for the first year of the study (2023). The diurnal variability has been examined separately for the two years to exclude the influence of growth rate on the diurnal amplitude. Figure S4 presents the diurnal variation for the second year of the study. All the seasons exhibit a similar diurnal pattern with maximum mole fraction in the early morning hours (05:00 - 08:00 am) and minimum mole fraction during the late afternoon hours (2:00 - 3:00 pm). Figure 7(e) shows the monthly average variation in diurnal amplitude during the study period. The difference between the maximum and minimum mole fraction of CO_2 in the diurnal cycle is defined as the diurnal amplitude. The diurnal amplitude shows large month-to-month variation with an increasing trend from May to September 2023 and a decreasing trend till February 2024. The lowest diurnal amplitude of about 29 ppm is observed in May, while the highest amplitude at about 63 ppm is observed in September/October (Figure 7(e)). We found that the post-monsoon season exhibited the highest diurnal variability (~ 60 ppm), followed by the pre-monsoon season (~ 35 ppm), winter season (~ 30 ppm) and the monsoon season (20 ppm). The same was observed for 2024 as well.

https://doi.org/10.5194/egusphere-2025-3538
Preprint. Discussion started: 29 September 2025

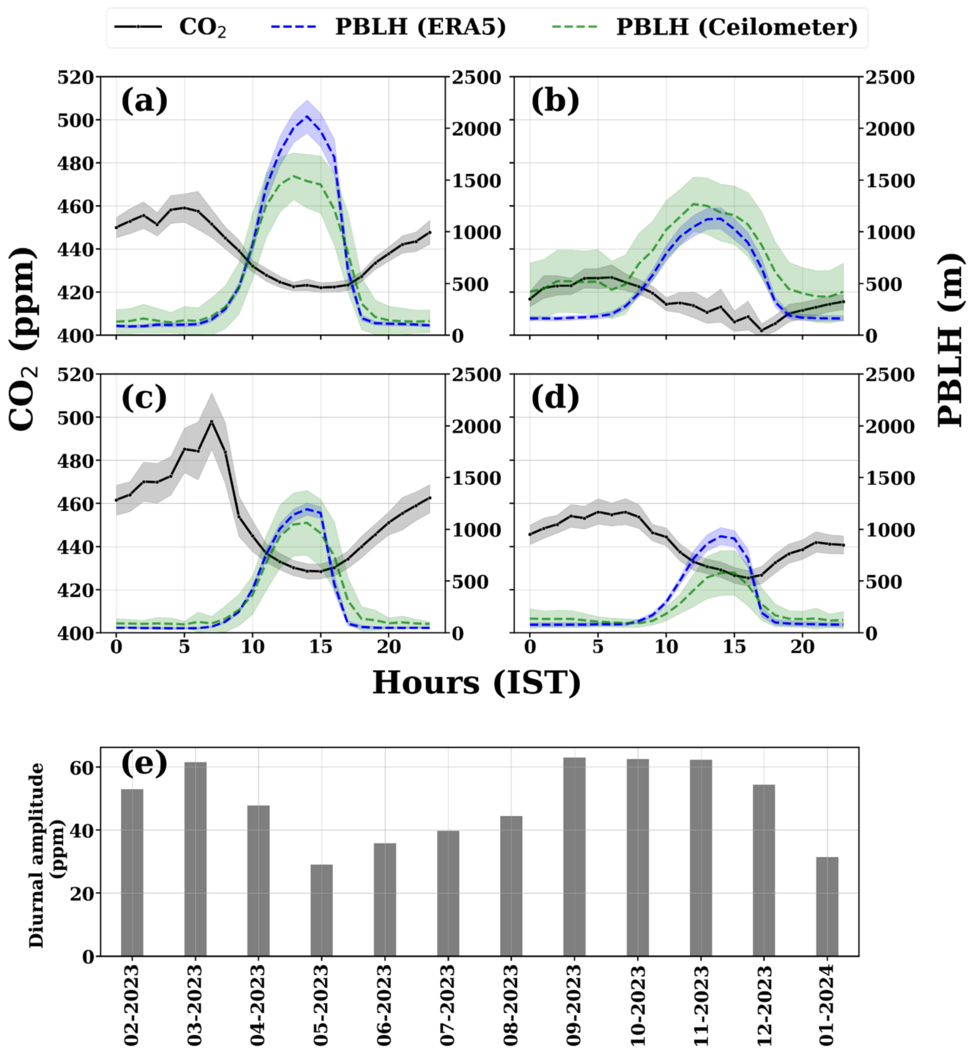

Figure 7: (a-d) Seasonally-averaged diurnal variation of atmospheric CO_2 over the Sonipat station during the pre-monsoon (MAM), monsoon (JJAS), post-monsoon (ON) and winter (DJF) seasons with planetary boundary layer heights (blue denotes PBLH from ERA5 and green denotes PBLH derived from Ceilometer), (e) monthly variation of the diurnal amplitude of CO_2 from February 2023 to January 2024.

The seasonal differences observed in the CO_2 diurnal amplitudes can be attributed to changes in local meteorology and biospheric activity over the monitoring station. A key factor that drives the diurnal variability of CO_2 is the PBLH, which depends on local meteorology.

https://doi.org/10.5194/egusphere-2025-3538
Preprint. Discussion started: 29 September 2025

The observed diurnal cycle of CO_2 is closely associated with the diurnal variation of the PBLH (Fig. 7). Figure S5 presents the seasonal variation of CO_2 compared with PBLH derived from Ceilometer and ERA5 reanalysis data. It is observed that the CO_2 mole fraction steadily increases throughout the night, reaching its peak in the early morning hours. This accumulation of CO_2 during the night-time can be attributed to poor mixing conditions due to shallow PBLH and biospheric respiration (Reid and Steyn, 1997). Similarly, minimum mole fraction are visible during the late afternoon hours (2:00 - 3:00 pm), irrespective of season, when the boundary layer is well mixed. The peak in CO_2 mole fraction during the morning hours can be attributed to the fumigation effect, a significant rise in surface pollutant mole fraction notable during the early morning hours due to the breakdown of the nocturnal inversion layer following sunrise (Stull, 1988). The fumigation effect is pronounced in the post-monsoon and winter seasons due to weak winds and a shallow PBLH.

Another key driver of CO_2 diurnal variability at Sonipat is the photosynthetic activity of the surrounding vegetation, a characteristic observed in rural areas with vegetative cover (Imasu & Tanabe, 2018). The combined effect of photosynthetic activity and a well-mixed PBLH (~1.3 km) during the afternoon hours in the post-monsoon season results in high diurnal variability. The low mole fraction during afternoon hours in the pre-monsoon season can be attributed to the dense PBLH (~ 2 km). The low diurnal variability during winter is due to the shallow PBLH (~ 900 m) and local meteorological conditions like weak winds. The delay in the evolution of the boundary layer could potentially result in a delayed, more pronounced fumigation peak during the winter season. Vegetative uptake of CO_2 is maximum during the monsoon season, and the poorly mixed PBL (~ 1.1 km) due to cloudy conditions contributes to minimum mole fraction and variability of CO_2 during this season. The diurnal variation of GHGs reported by several studies (Nishanth et al., 2014; Patil et al., 2014; Sharma et al., 2014) from different parts of the country shows a similar trend.

3.4 Drivers of CO_2 variability

The contribution of biospheric fluxes in driving the CO_2 mole fraction over Sonipat (for 2023) was analysed in Fig. 8. Figure 8(a) shows the simulated data from the Mi CASA biosphere model along with monthly averaged mole fraction of CO_2 and daytime CO_2 (06:00 – 18:00). The NEE flux represents the net carbon exchange between terrestrial ecosystems (difference between Rh and NPP). NPP is the net amount of CO_2 retained in the biosphere. Rh is the amount of CO_2 emitted into the atmosphere due to the decomposition of organic matter

https://doi.org/10.5194/egusphere-2025-3538
Preprint. Discussion started: 29 September 2025

by microorganisms in the soil. Figure 8(b) presents the simulated NEE from GEOS-Chem and GPP from FluxSat along with monthly averaged mole fraction of daily-mean and nighttime CO_2 (18:00 – 06:00). The GPP fluxes, a measure of carbon uptake by plants is also very high during this time. Reco the sum of Ra (autotrophic respiration) and Rh has been calculated as the difference of FluxSat GPP and GEOS-Chem NEE. Positive NEE values suggest an exchange of CO_2 from the biosphere to the atmosphere. On the other hand, a negative NEE value (when NPP exceeds Rh) suggests the uptake of CO_2 from the atmosphere to the biosphere.

The NEE flux presents a strong positive in June, followed by a gradual decrease up to October (monsoon). During this time, Reco, Rh and GPP exhibit strong enhancements. These enhancements are accompanied by the drawdown of CO_2 during this time. The driving factor for this drawdown of CO_2 during monsoon is the enhanced ecosystem productivity during this time. Interestingly, post-monsoon and winter months exhibit weak or negative NEE. This is because the Rh values are low during these seasons due to the drier soil conditions and the lack of soil moisture. It is also notable that GPP is very low during these months, which is associated with high CO_2 mole fraction as well. This increase in mole fraction is not only due to the lack of vegetation but also due to contributions from other local sources as well.

Figure 8(c) presents the correlation heatmap of all the variables. GPP, Rh and Reco exhibit an inverse correlation with CO_2. A strong inverse correlation of CO_2 with GPP suggests that the primary sink of CO_2 over Sonipat is biospheric activity. It is notable that GPP exhibits a strong positive correlation with Rh and Reco. This is due to the abundance of vegetation from the enhanced soil moisture during monsoon, suggesting that biospheric activity plays a key role in driving the CO_2 dynamics over Sonipat.

https://doi.org/10.5194/egusphere-2025-3538
Preprint. Discussion started: 29 September 2025

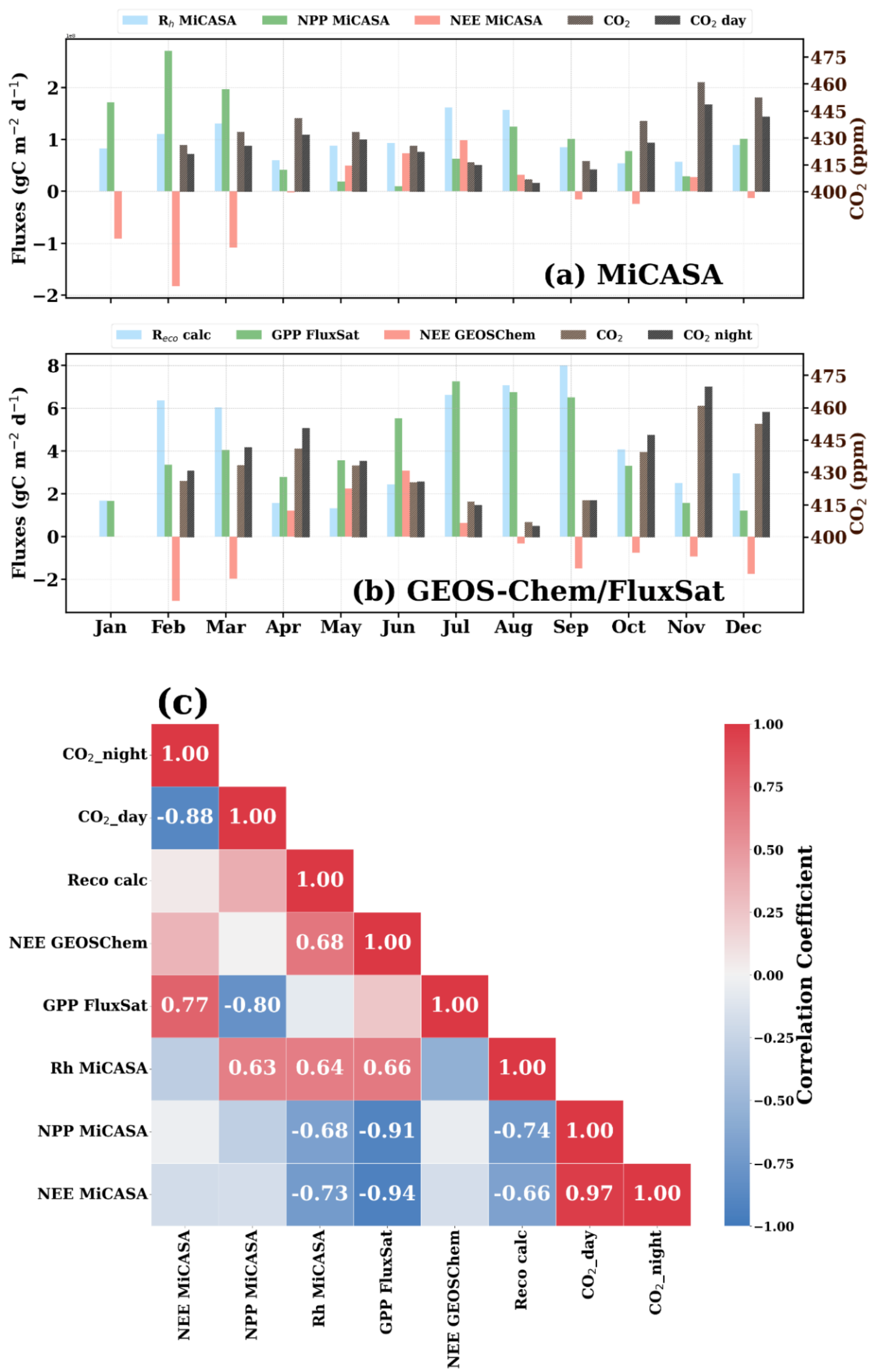

https://doi.org/10.5194/egusphere-2025-3538
Preprint. Discussion started: 29 September 2025

Figure 8: Monthly variation of atmospheric CO_2 mole fraction (for 2023) over the Sonipat monitoring station compared against (a) biospheric fluxes from the MiCASA terrestrial biospheric model and (b) GEOS-Chem model and FluxSat GPP data. (a - b) The CO_2 mole fraction are daytime-mean (06:00 - 18:00 LT) and night time-mean (18:00 - 06:00 LT). The correlation heatmap of all the variables. The annual growth rate of CO_2 has been subtracted from the CO_2 mole fraction using background data from the Mauna Lou observatory. The variable "Reco calc" was calculated as the difference between NEE (GEOS-Chem) and GPP (FluxSat). The Pearson correlation coefficients with a p value less than 0.05 have been displayed in the correlation plot.

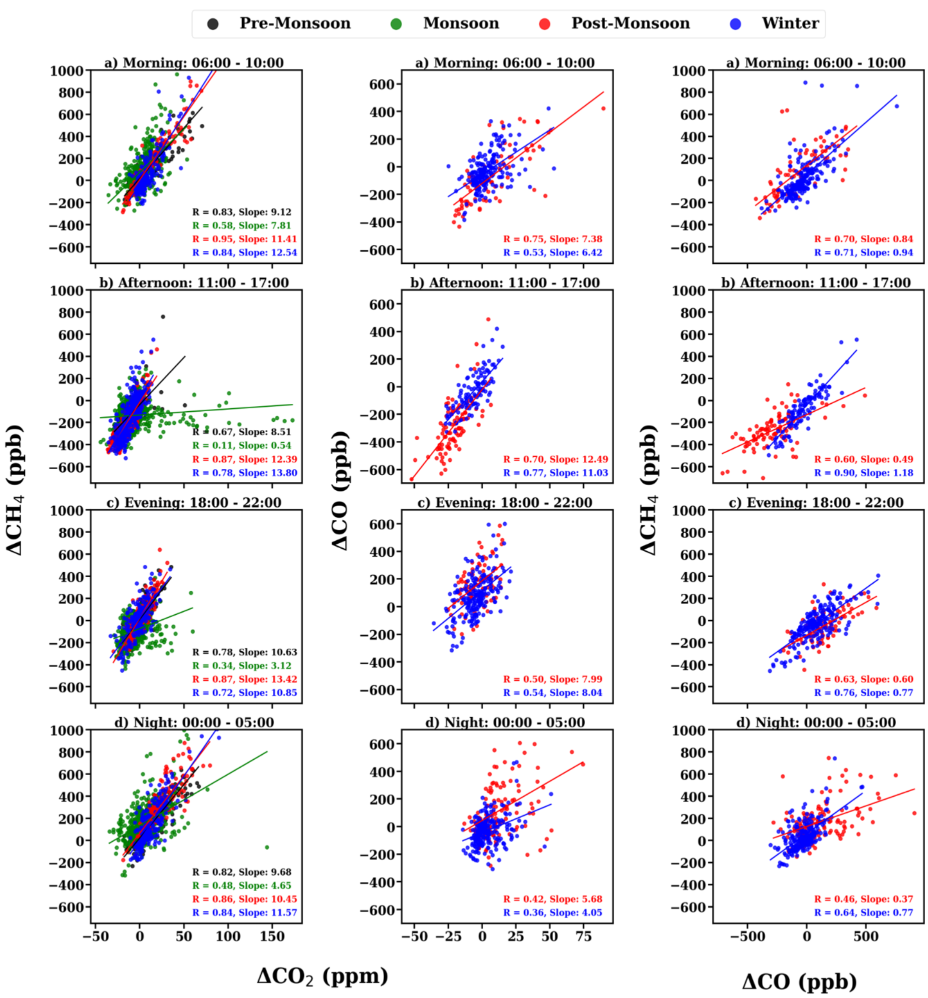

https://doi.org/10.5194/egusphere-2025-3538
Preprint. Discussion started: 29 September 2025

Figure 9: Tracer to tracer relations of ΔCO_2 / ΔCH_4 (left panel), ΔCO_2 / ΔCO (middle panel) and ΔCH_4 / ΔCO (right panel) during a) Morning (0600–1000 IST), b) afternoon (1100–1700 IST), c) evening (1800–2200 IST) and d) night (0000–0500 IST).

3.5 Tracer-Tracer relationships

The ratios (tracer-tracer) of GHGs have been widely used in previous studies to estimate different emission source contributions to atmospheric GHGs (Chandra et al., 2016, 2019; Lin et al., 2015; Lopez, 2012; Paris et al., 2008; Sreenivas et al., 2016, 2022). We follow a similar tracer-tracer correlation analysis though the stations are in different geographical locations, however this will help to assess the synoptic variation of CO_2 at different diurnal time windows to understand the emission sources contributing to CO_2 mole fraction over Sonipat (Fig. 9). The measurements have been divided into four-time windows: (a) morning hours (06:00 - 10:00; the PBLH starts to develop after sunrise; local traffic is high), (b) afternoon hours (11:00 - 17:00; the PBLH is well-developed; relatively minimum local traffic, (c) evening hours (18:00 - 22:00; rush hour traffic and high household emissions), and (d) night hours (00:00 - 00:05; relatively less anthropogenic emission sources). Excessive mole fraction were used in the correlation analysis to remove the influence of background mole fraction on the correlation ratios (Worthy et al., 2009). The correlation between the different gases (CO_2, CH_4, and CO) has been studied using the robust linear fit regression method.

3.5.1 Correlation between CO_2 and CH_4

Figure 9 (left panel) presents the correlation of excess mole fraction of CH_4 and CO_2 during the four seasons. The CH_4/CO_2 correlation reveals a strong correlation ($r > 0.6$) for all seasons except monsoon during all time windows, which suggests a similar source mechanism or a controlling emission process for both gases at the measurement site. Around the study location, vehicular emissions from the nearby highway and natural gas combustion emissions are possible sources. Also, a positive correlation suggests the dominance of anthropogenic emissions on the carbon cycle over Sonipat (Fang et al., 2015). During monsoon season, the afternoon time window has a weak correlation with other time windows, revealing the different source and sink mechanisms of CO_2 and CH_4, such as the loss of CH_4 by hydroxyl radical and the uptake of CO_2 by plants. The regression slope exhibits a higher slope during the post-monsoon and winter months, and this is associated with the lack of photosynthetic activity and the dominance of local emissions and long-range transport. The lower values during pre-monsoon and monsoon seasons are associated with the dominance of vegetation and

https://doi.org/10.5194/egusphere-2025-3538
Preprint. Discussion started: 29 September 2025

photosynthetic activity (terrestrial uptake of CO_2). The regression slope shows strong diurnal variation throughout all seasons. Similar studies across India have presented similar results with high regression slopes during post-monsoon and winter in comparison to pre-monsoon and monsoon seasons (Lin et al., 2015; Sreenivas et al., 2016, 2022).

3.5.2 Correlation between CO_2 and CO

Figure 9 (middle panel) presents the correlation of excess mole fraction of CO and CO_2 during post-monsoon and winter seasons. The CO/CO_2 correlation shows strong diurnal variability suggesting the dominance of different source mechanisms throughout the day, with strong correlation during the morning and afternoon hours (suggesting a similar source) and a weaker correlation during the evening and night hours (suggesting different sources) between these gases. The postmonsoon season has higher regression slopes, which can be associated with the lack of photosynthetic activity combined with the crop residue burning. The CO/CO_2 ratio over Sonipat (4 – 12.5 ppb ppm^{-1}) is lower than those for fresh plumes from wildfire (Andreae and Merlet, 2001; Mauzerall et al., 1998) and much lower than that from biomass burning events (Matsueda et al., 1999). The low ratios of CO/CO_2 can also be due to the contribution of biofuel burning (which has a higher burning efficiency) during post-monsoon and winter (Andreae and Merlet, 2001). Lin et al. (2015) reported CO/CO_2 ratios of 13 ppb ppm^{-1} over Southeast Asian outflow from February to April 2001. This value was suggested to be not only due to biomass/biofuel burning but also due to fossil fuel emissions (Russo et al., 2003), crop residue burning, and biofuel burning have a combined influence on CO_2 and CO mole fraction over Sonipat during post monsoon and winter. Although there is a contribution of CO and CO_2 from long-range airmass transport (influence of crop residue burning over Punjab) from the northwest side of the monitoring station, the effect is diluted by other sources. Figure S2 presents the wind patterns during the different seasons, revealing the predominant winds from the northwest during the post-monsoon season.

3.5.3 Correlation between CH_4 and CO

Figure 9 (right panel) presents the correlation of excess mole fraction of CH_4 and CO during post-monsoon and winter seasons. The CH_4/CO correlation reveals a stronger correlation ($r > 0.7$) during winter compared to post-monsoon during all time windows, which suggests similar sources during winter, and a relatively weaker correlation in post-monsoon reveals different sources. The regression slope exhibits a higher slope during winter compared to post-monsoon. This is associated with the lack of photosynthetic activity and the dominance of local emissions

https://doi.org/10.5194/egusphere-2025-3538
Preprint. Discussion started: 29 September 2025

and long-range transport. The CH_4/CO ratios range from 0.3 to 1.2 over Sonipat, indicative of anthropogenic emission sources (Bakwin et al., 1995; Harriss et al., 1994; Lai et al., 2010; Lin et al., 2015; Niwa et al., 2012; Sawa et al., 2004; Wada et al., 2011; Xiao et al., 2004). The CH_4/CO ratios range of 0.07 – 0.3 indicates the contribution from biomass and biofuel burning (Andreae and Merlet, 2001; Mauzerall et al., 1998; Mühle et al., 2002).

Lin et al. (2015) presented similar ratios of CH_4/CO over Pondicherry (PON) and Port Blair (PBL). High CH_4 emissions from livestock can raise the low CH_4/CO ratios from biomass burning. CH_4 and CO emissions from biomass, biofuel burning and livestock estimated from EDGAR v4.2, 2011 indicate a CH_4/CO ratio of 0.64 – 0.69 over the Indian subcontinent from 2000-2008. These ratios are comparable to the ratios observed during both seasons over Sonipat.

4. Conclusions

This study investigated the high temporal variability of atmospheric CO_2 mole fraction at Sonipat, a suburban station in the Indo-Gangetic Plain. Sonipat's location, being in the downwind of Punjab and upwind of Delhi, makes it an ideal site for examining the influence of different regional air masses in the IGP region. The atmospheric CO_2 mole fraction from February 2023 to January 2025 have been measured with a GHG analyser using the laser-based cavity ring-down spectroscopy technique. To understand the key drivers of seasonal and diurnal CO_2 variability over the Sonipat station and the IGP region, we used a combination of ground-based and satellite-based measurements, three different model outputs, ecosystem proxy variables, and tracer-tracer analysis technique.

The salient findings from this study are listed below.

- The surface-based measurements of atmospheric CO_2 mole fraction exhibit the large CO_2 seasonality with maximum mole fraction (456.4 ppm) during post-monsoon and minimum mole fraction (407.2 ppm) during monsoon, with an average mole fraction of 422.6 ppm.
- The comparison of the seasonality of atmospheric CO_2 over Sonipat with other Indian and global sites in the same latitudinal band reveals very high seasonality over that is observed at Sonipat. This high seasonality is attributed to the high mole fraction of CO_2 during November (post-monsoon) from local emissions and crop residue burning. The location of the measurement site in the IGP region on the downwind of Punjab is a major reason for this strong seasonal variability compared to other sites in the same latitudinal band.

https://doi.org/10.5194/egusphere-2025-3538
Preprint. Discussion started: 29 September 2025

- Our results also indicate that the biospheric activity was the primary driver of CO_2 seasonal variability over Sonipat, with anthropogenic emissions and soil respiration as the major sources and photosynthetic carbon uptake as the major sink. In addition, the boundary layer dynamics and air mass transport from upwind regions significantly contribute to the build-up of CO_2 mole fraction.
- Although both the CarbonTracker and MIROC-ACTM models could capture the broad seasonal pattern of CO_2 mole fraction, the models substantially underestimated the CO_2 mole fraction. The OCO-2 and OCO-3 satellite XCO_2 retrievals also revealed similar seasonal variability; however, the satellites could not capture CO_2 enhancements due to local sources.
- The atmospheric CO_2 mole fraction at Sonipat exhibit a consistent diurnal pattern irrespective of season, with an observed maximum during morning hours, which can be attributed to the fumigation effect, with a gradual decrease during the day and a minimum during afternoon hours with enhanced photosynthetic activity. A slight shift in time for the morning peaks was observed from season to season due to the change in the time of sunrise, resulting in a shift in photosynthetic activity. The diurnal amplitude of CO_2 was observed to peak in post-monsoon (maximum in November) and draw down (minimum in May) in monsoon.
- The tracer-tracer relationships during different time periods for the post-monsoon and winter seasons were examined. Analysis reveals that CO_2 and CH_4 show a strong positive correlation during all seasons, and the higher slopes are due to the lack of photosynthetic activity and the influence of local winds. This strong correlation suggests common anthropogenic sources for both these gases. The CO/CO_2 ratios reveal the influence of long-range transport of crop residue burning over Punjab on CO_2 mole fraction in Sonipat during post-monsoon.

https://doi.org/10.5194/egusphere-2025-3538
Preprint. Discussion started: 29 September 2025

Data availability

- The OCO-2 and OCO-3 data is downloaded from https://disc.gsfc.nasa.gov/datasets/. This study utilizes the bias-corrected OCO-2 v11.1r data product (https://disc.gsfc.nasa.gov/datasets/OCO2_L2_Lite_FP_11.1r/summary?keywords=oco2) and the OCO-3 v10.4r data product (https://disc.gsfc.nasa.gov/datasets/OCO3_L2_Lite_FP_10.4r/summary?keywords=oco3).
- The CT-2020 model outputs were downloaded from https://gml.noaa.gov/aftp/products/carbontracker/co2/. The CASA model outputs were downloaded from https://disc.gsfc.nasa.gov/datasets/GEOS_CASAGFED_M_FLUX_3/summary?keywords=CASA.
- The ERA5 reanalysis datasets were downloaded from https://cds.climate.copernicus.eu/cdsapp#!/dataset/reanalysis-era5-single-levels.
- The satellite estimates of NDVI were downloaded from https://www.ncei.noaa.gov/data/land-normalized-difference-vegetation-index/access/.
- This study utilises bias-corrected SIF data from OCO-2 v11r data product (https://disc.gsfc.nasa.gov/datasets/OCO2_L2_Lite_SIF_11r/summary?keywords=oco2%20sif).
- The FluxSat data is downloaded from https://avdc.gsfc.nasa.gov/pub/tmp/FluxSat_GPP/. This study uses FluxSat version 2.2 dataproduct.
- The ObsPack data is available at https://gml.noaa.gov/ccgg/obspack/data.php. This study used ObsPack V2.0 dataproduct.

Acknowledgements:

We acknowledge institutional support and funding provided by IIT Delhi and other stakeholders to develop the IIT Delhi Atmospheric Observatory at Sonipat. In particular, we thank Shahzad Gani (IIT Delhi) for his contribution to the observatory. We thank the Aakash Project team for providing trace gas data from the CUPI-G sensors. We acknowledge the OCO-2, OCO-3, CASA, CarbonTracker, and ERA5 teams for providing the data used in this study.

https://doi.org/10.5194/egusphere-2025-3538
Preprint. Discussion started: 29 September 2025

Author Contributions:

Conceptualization: VJV, RKK, SP

Data curation: VJV, RKK, JR, DG, SD, YM, PKP

Investigation, Methodology: VJV, RKK, SP, PKP

Software, Visualisation: VJV

Writing – original draft: VJV

Writing – review & editing: RKK, JR, DG, SD, YM, PKP

Competing interests

The authors declare that they have no conflict of interest.

https://doi.org/10.5194/egusphere-2025-3538
Preprint. Discussion started: 29 September 2025

References

Aburas, M. M., Abdullah, S. H., Ramli, M. F., and Ash'aari, Z. H.: Measuring Land Cover Change in Seremban, Malaysia Using NDVI Index, Procedia Environmental Sciences, 30, 238–243, https://doi.org/10.1016/j.proenv.2015.10.043, 2015.

Ammoura, L., Xueref-Remy, I., Gros, V., Baudic, A., Bonsang, B., Petit, J.-E., Perrussel, O., Bonnaire, N., Sciare, J., and Chevallier, F.: Atmospheric measurements of ratios between CO₂ and co-emitted species from traffic: a tunnel study in the Paris megacity, Atmos. Chem. Phys., 14, 12871–12882, https://doi.org/10.5194/acp-14-12871-2014, 2014.

Andreae, M. O. and Merlet, P.: Emission of trace gases and aerosols from biomass burning, Global Biogeochemical Cycles, 15, 955–966, https://doi.org/10.1029/2000GB001382, 2001.

Apadula, F., Cassardo, C., Ferrarese, S., Heltai, D., and Lanza, A.: Thirty Years of Atmospheric CO2 Observations at the Plateau Rosa Station, Italy, Atmosphere, 10, 418, https://doi.org/10.3390/atmos10070418, 2019.

Baars, H., Ansmann, A., Engelmann, R., and Althausen, D.: Continuous monitoring of the boundary-layer top with lidar, Atmospheric Chemistry and Physics, 8, 7281–7296, https://doi.org/10.5194/acp-8-7281-2008, 2008.

Baker, A. K., Schuck, T. J., Brenninkmeijer, C. A. M., Rauthe-Schöch, A., Slemr, F., van Velthoven, P. F. J., and Lelieveld, J.: Estimating the contribution of monsoon-related biogenic production to methane emissions from South Asia using CARIBIC observations, Geophysical Research Letters, 39, https://doi.org/10.1029/2012GL051756, 2012.

Bakwin, P. S., Tans, P. S., Zhao, C., Ussler III, W., and Quesnell, E.: Measurements of carbon dioxide on a very tall tower, Tellus B: Chemical and Physical Meteorology, 47, 535–549, https://doi.org/10.3402/tellusb.v47i5.16070, 1995.

Bhattacharya, S. K., Borole, D. V., Francy, R. J., Allison, C. E., Steele, L. P., Krummel, P., Langenfelds, R., Masarie, K. A., Tiwari, Y. K., and Patra, P. K.: Trace gases and CO_2 isotope records from Cabo de Rama, India, Current Science, 97, 1336–1344, 2009.

Bisht, J. S. H., Machida, T., Chandra, N., Tsuboi, K., Patra, P. K., Umezawa, T., Niwa, Y., Sawa, Y., Morimoto, S., Nakazawa, T., Saitoh, N., and Takigawa, M.: Seasonal Variations of SF_6 , CO_2 , CH_4 , and N_2 O in the UT/LS Region due to Emissions, Transport, and Chemistry, JGR Atmospheres, 126, e2020JD033541, https://doi.org/10.1029/2020JD033541, 2021.

Brad Weir (2024), MiCASA Daily NPP Rh Fire Fuel Fluxes 0.1 degree × 0.1 degree V1, Greenbelt, MD, USA, NASA Center for Climate Simulation (NCCS) DataPortal, Accessed: [March 20, 2025], 10.5067/ZBXSA1LEN453

Byrne, B., Jones, D. B. A., Strong, K., Zeng, Z. -C., Deng, F., and Liu, J.: Sensitivity of CO_2 surface flux constraints to observational coverage, JGR Atmospheres, 122, 6672–6694, https://doi.org/10.1002/2016JD026164, 2017.

Campbell, J. E., Carmichael, G. R., Chai, T., Mena-Carrasco, M., Tang, Y., Blake, D. R., Blake, N. J., Vay, S. A., Collatz, G. J., Baker, I., Berry, J. A., Montzka, S. A., Sweeney, C.,

https://doi.org/10.5194/egusphere-2025-3538
Preprint. Discussion started: 29 September 2025

Schnoor, J. L., and Stanier, C. O.: Photosynthetic Control of Atmospheric Carbonyl Sulfide During the Growing Season, Science, 322, 1085–1088, https://doi.org/10.1126/science.1164015, 2008.

Chakraborty, S., Tiwari, Y. K., Deb Burman, P. K., Baidya Roy, S., and Valsala, V.: Observations and Modeling of GHG Concentrations and Fluxes Over India, in: Assessment of Climate Change over the Indian Region: A Report of the Ministry of Earth Sciences (MoES), Government of India, edited by: Krishnan, R., Sanjay, J., Gnanaseelan, C., Mujumdar, M., Kulkarni, A., and Chakraborty, S., Springer, Singapore, 73–92, https://doi.org/10.1007/978-981-15-4327-2_4, 2020.

Chandra, N., Lal, S., Venkataramani, S., Patra, P. K., and Sheel, V.: Temporal variations of atmospheric CO₂ and CO at Ahmedabad in western India, Atmos. Chem. Phys., 16, 6153–6173, https://doi.org/10.5194/acp-16-6153-2016, 2016.

Chandra, N., Venkataramani, S., Lal, S., Patra, P. K., Ramonet, M., Lin, X., and Sharma, S. K.: Observational evidence of high methane emissions over a city in western India, Atmospheric Environment, 202, 41–52, https://doi.org/10.1016/j.atmosenv.2019.01.007, 2019.

Chandra, N., Patra, P. K., Bisht, J. S. H., Ito, A., Umezawa, T., Saigusa, N., Morimoto, S., Aoki, S., Janssens-Maenhout, G., Fujita, R., Takigawa, M., Watanabe, S., Saitoh, N., and Canadell, J. G.: Emissions from the Oil and Gas Sectors, Coal Mining and Ruminant Farming Drive Methane Growth over the Past Three Decades, Journal of the Meteorological Society of Japan, 99, 309–337, https://doi.org/10.2151/jmsj.2021-015, 2021.

Chandra, N., Patra, P. K., Niwa, Y., Ito, A., Iida, Y., Goto, D., Morimoto, S., Kondo, M., Takigawa, M., Hajima, T., and Watanabe, M.: Estimated regional CO_2 flux and uncertainty based on an ensemble of atmospheric CO_2 inversions, Atmos. Chem. Phys., 22, 9215–9243, https://doi.org/10.5194/acp-22-9215-2022, 2022.

Chen, H., Karion, A., Rella, C. W., Winderlich, J., Gerbig, C., Filges, A., Newberger, T., Sweeney, C., and Tans, P. P.: Accurate measurements of carbon monoxide in humid air using the cavity ring-down spectroscopy (CRDS) technique, Atmospheric Measurement Techniques, 6, 1031–1040, https://doi.org/10.5194/amt-6-1031-2013, 2013.

Chen, Y., Hall, J., Van Wees, D., Andela, N., Hantson, S., Giglio, L., Van Der Werf, G. R., Morton, D. C., and Randerson, J. T.: Multi-decadal trends and variability in burned area from the fifth version of the Global Fire Emissions Database (GFED5), Earth Syst. Sci. Data, 15, 5227–5259, https://doi.org/10.5194/essd-15-5227-2023, 2023.

Crisp, D., Pollock, H. R., Rosenberg, R., Chapsky, L., Lee, R. A. M., Oyafuso, F. A., Frankenberg, C., O'Dell, C. W., Bruegge, C. J., Doran, G. B., Eldering, A., Fisher, B. M., Fu, D., Gunson, M. R., Mandrake, L., Osterman, G. B., Schwandner, F. M., Sun, K., Taylor, T. E., Wennberg, P. O., and Wunch, D.: The on-orbit performance of the Orbiting Carbon Observatory-2 (OCO-2) instrument and its radiometrically calibrated products, Atmos. Meas. Tech., 10, 59–81, https://doi.org/10.5194/amt-10-59-2017, 2017.

Das, C., Kunchala, R. K., Chandra, N., Chhabra, A., and Pandya, M. R.: Characterizing the regional XCO2 variability and its association with ENSO over India inferred from GOSAT

https://doi.org/10.5194/egusphere-2025-3538
Preprint. Discussion started: 29 September 2025

and OCO-2 satellite observations, Science of The Total Environment, 902, 166176, https://doi.org/10.1016/j.scitotenv.2023.166176, 2023.

Eldering, A., O'Dell, C. W., Wennberg, P. O., Crisp, D., Gunson, M. R., Viatte, C., Avis, C., Braverman, A., Castano, R., Chang, A., Chapsky, L., Cheng, C., Connor, B., Dang, L., Doran, G., Fisher, B., Frankenberg, C., Fu, D., Granat, R., Hobbs, J., Lee, R. A. M., Mandrake, L., McDuffie, J., Miller, C. E., Myers, V., Natraj, V., O'Brien, D., Osterman, G. B., Oyafuso, F., Payne, V. H., Pollock, H. R., Polonsky, I., Roehl, C. M., Rosenberg, R., Schwandner, F., Smyth, M., Tang, V., Taylor, T. E., To, C., Wunch, D., and Yoshimizu, J.: The Orbiting Carbon Observatory-2: first 18 months of science data products, Atmos. Meas. Tech., 10, 549–563, https://doi.org/10.5194/amt-10-549-2017, 2017.

Eldering, A., Taylor, T. E., O'Dell, C. W., and Pavlick, R.: The OCO-3 mission: measurement objectives and expected performance based on 1 year of simulated data, Atmos. Meas. Tech., 12, 2341–2370, https://doi.org/10.5194/amt-12-2341-2019, 2019.

Fang, S. X., Tans, P. P., Steinbacher, M., Zhou, L. X., and Luan, T.: Comparison of the regional CO_2 mole fraction filtering approaches at a WMO/GAW regional station in China, Atmospheric Measurement Techniques, 8, 5301–5313, https://doi.org/10.5194/amt-8-5301-2015, 2015.

Fawzy, S., Osman, A. I., Doran, J., and Rooney, D. W.: Strategies for mitigation of climate change: a review, Environ Chem Lett, 18, 2069–2094, https://doi.org/10.1007/s10311-020-01059-w, 2020.

Frankenberg, C., O'Dell, C., Berry, J., Guanter, L., Joiner, J., Köhler, P., Pollock, R., and Taylor, T. E.: Prospects for chlorophyll fluorescence remote sensing from the Orbiting Carbon Observatory-2, Remote Sensing of Environment, 147, 1–12, https://doi.org/10.1016/j.rse.2014.02.007, 2014.

Friedlingstein, P., O'Sullivan, M., Jones, M. W., Andrew, R. M., Hauck, J., Landschützer, P., Le Quéré, C., Li, H., Luijkx, I. T., Olsen, A., Peters, G. P., Peters, W., Pongratz, J., Schwingshackl, C., Sitch, S., Canadell, J. G., Ciais, P., Jackson, R. B., Alin, S. R., Arneth, A., Arora, V., Bates, N. R., Becker, M., Bellouin, N., Berghoff, C. F., Bittig, H. C., Bopp, L., Cadule, P., Campbell, K., Chamberlain, M. A., Chandra, N., Chevallier, F., Chini, L. P., Colligan, T., Decayeux, J., Djeutchouang, L. M., Dou, X., Duran Rojas, C., Enyo, K., Evans, W., Fay, A. R., Feely, R. A., Ford, D. J., Foster, A., Gasser, T., Gehlen, M., Gkritzalis, T., Grassi, G., Gregor, L., Gruber, N., Gürses, Ö., Harris, I., Hefner, M., Heinke, J., Hurtt, G. C., Iida, Y., Ilyina, T., Jacobson, A. R., Jain, A. K., Jarníková, T., Jersild, A., Jiang, F., Jin, Z., Kato, E., Keeling, R. F., Klein Goldewijk, K., Knauer, J., Korsbakken, J. I., Lan, X., Lauvset, S. K., Lefèvre, N., Liu, Z., Liu, J., Ma, L., Maksyutov, S., Marland, G., Mayot, N., McGuire, P. C., Metzl, N., Monacci, N. M., Morgan, E. J., Nakaoka, S.-I., Neill, C., Niwa, Y., Nützel, T., Olivier, L., Ono, T., Palmer, P. I., Pierrot, D., Qin, Z., Resplandy, L., Roobaert, A., Rosan, T. M., Rödenbeck, C., Schwinger, J., Smallman, T. L., Smith, S. M., Sospedra-Alfonso, R., Steinhoff, T., et al.: Global Carbon Budget 2024, Earth Syst. Sci. Data, 17, 965–1039, https://doi.org/10.5194/essd-17-965-2025, 2025.

Hammerling, D. M., Michalak, A. M., O'Dell, C., and Kawa, S. R.: Global CO_2 distributions over land from the Greenhouse Gases Observing Satellite (GOSAT), Geophysical Research Letters, 39, 2012GL051203, https://doi.org/10.1029/2012GL051203, 2012.

https://doi.org/10.5194/egusphere-2025-3538
Preprint. Discussion started: 29 September 2025

Harriss, R. C., Sachse, G. W., Collins Jr., J. E., Wade, L., Bartlett, K. B., Talbot, R. W., Browell, E. V., Barrie, L. A., Hill, G. F., and Burney, L. G.: Carbon monoxide and methane over Canada: July–August 1990, Journal of Geophysical Research: Atmospheres, 99, 1659–1669, https://doi.org/10.1029/93JD01906, 1994.

Huang, J., Golombek, A., Prinn, R., Weiss, R., Fraser, P., Simmonds, P., Dlugokencky, E. J., Hall, B., Elkins, J., Steele, P., Langenfelds, R., Krummel, P., Dutton, G., and Porter, L.: Estimation of regional emissions of nitrous oxide from 1997 to 2005 using multinetwork measurements, a chemical transport model, and an inverse method, Journal of Geophysical Research: Atmospheres, 113, https://doi.org/10.1029/2007JD009381, 2008.

Huang, J., Yu, H., Guan, X., Wang, G., and Guo, R.: Accelerated dryland expansion under climate change, Nature Clim Change, 6, 166–171, https://doi.org/10.1038/nclimate2837, 2016.

IPCC, 2021: Climate Change 2021: The Physical Science Basis. Contribution of Working Group I to the Sixth Assessment Report of the Intergovernmental Panel on Climate Change[Masson-Delmotte, V., P. Zhai, A. Pirani, S.L. Connors, C. Péan, S. Berger, N. Caud, Y. Chen, L. Goldfarb, M.I. Gomis, M. Huang, K. Leitzell, E. Lonnoy, J.B.R. Matthews, T.K. Maycock, T. Waterfield, O. Yelekçi, R. Yu, and B. Zhou (eds.)]. Cambridge University Press, Cambridge, United Kingdom and New York, NY, USA, In press, doi:10.1017/9781009157896.

Ito, A.: Disequilibrium of terrestrial ecosystem CO_2 budget caused by disturbance-induced emissions and non-CO_2 carbon export flows: a global model assessment, Earth Syst. Dynam., 10, 685–709, https://doi.org/10.5194/esd-10-685-2019, 2019.

Jain, C. D., Singh, V., Akhil Raj, S. T., Madhavan, B. L., and Ratnam, M. V.: Local emission and long-range transport impacts on the CO, CO2, and CH4 concentrations at a tropical rural site, Atmospheric Environment, 254, 118397, https://doi.org/10.1016/j.atmosenv.2021.118397, 2021.

Jing, X., Huang, J., Wang, G., Higuchi, K., Bi, J., Sun, Y., Yu, H., and Wang, T.: The effects of clouds and aerosols on net ecosystem CO_2 exchange over semi-arid Loess Plateau of Northwest China, Atmospheric Chemistry and Physics, 10, 8205–8218, https://doi.org/10.5194/acp-10-8205-2010, 2010.

Joiner, J. and Yoshida, Y.: Satellite-based reflectances capture large fraction of variability in global gross primary production (GPP) at weekly time scales, Agricultural and Forest Meteorology, 291, 108092, https://doi.org/10.1016/j.agrformet.2020.108092, 2020.

Joiner, J., Yoshida, Y., Zhang, Y., Duveiller, G., Jung, M., Lyapustin, A., Wang, Y., and Tucker, C. J.: Estimation of Terrestrial Global Gross Primary Production (GPP) with Satellite Data-Driven Models and Eddy Covariance Flux Data, Remote Sensing, 10, 1346, https://doi.org/10.3390/rs10091346, 2018.

Jones, M. W., Andrew, R. M., Peters, G. P., Janssens-Maenhout, G., De-Gol, A. J., Ciais, P., Patra, P. K., Chevallier, F., and Le Quéré, C.: Gridded fossil CO2 emissions and related O2 combustion consistent with national inventories 1959–2018, Sci Data, 8, 2, https://doi.org/10.1038/s41597-020-00779-6, 2021.

https://doi.org/10.5194/egusphere-2025-3538
Preprint. Discussion started: 29 September 2025

Kar, J., Bremer, H., Drummond, J. R., Rochon, Y. J., Jones, D. B. A., Nichitiu, F., Zou, J., Liu, J., Gille, J. C., Edwards, D. P., Deeter, M. N., Francis, G., Ziskin, D., and Warner, J.: Evidence of vertical transport of carbon monoxide from Measurements of Pollution in the Troposphere (MOPITT), Geophysical Research Letters, 31, https://doi.org/10.1029/2004GL021128, 2004.

Kawa, S. R., Mao, J., Abshire, J. B., Collatz, G. J., Sun, X., and Weaver, C. J.: Simulation studies for a space-based CO_2 lidar mission, Tellus B: Chemical and Physical Meteorology, 62, 759, https://doi.org/10.1111/j.1600-0889.2010.00486.x, 2010.

Kirschke, S., Bousquet, P., Ciais, P., Saunois, M., Canadell, J. G., Dlugokencky, E. J., Bergamaschi, P., Bergmann, D., Blake, D. R., Bruhwiler, L., Cameron-Smith, P., Castaldi, S., Chevallier, F., Feng, L., Fraser, A., Heimann, M., Hodson, E. L., Houweling, S., Josse, B., Fraser, P. J., Krummel, P. B., Lamarque, J.-F., Langenfelds, R. L., Le Quéré, C., Naik, V., O'Doherty, S., Palmer, P. I., Pison, I., Plummer, D., Poulter, B., Prinn, R. G., Rigby, M., Ringeval, B., Santini, M., Schmidt, M., Shindell, D. T., Simpson, I. J., Spahni, R., Steele, L. P., Strode, S. A., Sudo, K., Szopa, S., van der Werf, G. R., Voulgarakis, A., van Weele, M., Weiss, R. F., Williams, J. E., and Zeng, G.: Three decades of global methane sources and sinks, Nature Geosci, 6, 813–823, https://doi.org/10.1038/ngeo1955, 2013.

Krol, M., Houweling, S., Bregman, B., van den Broek, M., Segers, A., van Velthoven, P., Peters, W., Dentener, F., and Bergamaschi, P.: The two-way nested global chemistry-transport zoom model TM5: algorithm and applications, Atmospheric Chemistry and Physics Discussions, 4, 3975–4018, 2004.

Kumar, A., Yu, Z.-G., Klemeš, J. J., and Bokhari, A.: A state-of-the-art review of greenhouse gas emissions from Indian hydropower reservoirs, Journal of Cleaner Production, 320, 128806, https://doi.org/10.1016/j.jclepro.2021.128806, 2021.

Kunchala, R. K., Patra, P. K., Kumar, K. N., Chandra, N., Attada, R., and Karumuri, R. K.: Spatio-temporal variability of XCO2 over Indian region inferred from Orbiting Carbon Observatory (OCO-2) satellite and Chemistry Transport Model, Atmospheric Research, 269, 106044, https://doi.org/10.1016/j.atmosres.2022.106044, 2022.

Kuttippurath, J., Peter, R., Singh, A., and Raj, S.: The increasing atmospheric CO2 over India: Comparison to global trends, iScience, 25, 104863, https://doi.org/10.1016/j.isci.2022.104863, 2022.

Lai, S. C., Baker, A. K., Schuck, T. J., van Velthoven, P., Oram, D. E., Zahn, A., Hermann, M., Weigelt, A., Slemr, F., Brenninkmeijer, C. a. M., and Ziereis, H.: Pollution events observed during CARIBIC flights in the upper troposphere between South China and the Philippines, Atmospheric Chemistry and Physics, 10, 1649–1660, https://doi.org/10.5194/acp-10-1649-2010, 2010.

Le Quéré, C., Andrew, R. M., Friedlingstein, P., Sitch, S., Pongratz, J., Manning, A. C., Korsbakken, J. I., Peters, G. P., Canadell, J. G., Jackson, R. B., Boden, T. A., Tans, P. P., Andrews, O. D., Arora, V. K., Bakker, D. C. E., Barbero, L., Becker, M., Betts, R. A., Bopp, L., Chevallier, F., Chini, L. P., Ciais, P., Cosca, C. E., Cross, J., Currie, K., Gasser, T., Harris, I., Hauck, J., Haverd, V., Houghton, R. A., Hunt, C. W., Hurtt, G., Ilyina, T., Jain, A. K., Kato, E., Kautz, M., Keeling, R. F., Klein Goldewijk, K., Körtzinger, A., Landschützer, P., Lefèvre, N., Lenton, A., Lienert, S., Lima, I., Lombardozzi, D., Metzl, N., Millero, F.,

https://doi.org/10.5194/egusphere-2025-3538
Preprint. Discussion started: 29 September 2025

Monteiro, P. M. S., Munro, D. R., Nabel, J. E. M. S., Nakaoka, S., Nojiri, Y., Padin, X. A., Peregon, A., Pfeil, B., Pierrot, D., Poulter, B., Rehder, G., Reimer, J., Rödenbeck, C., Schwinger, J., Séférian, R., Skjelvan, I., Stocker, B. D., Tian, H., Tilbrook, B., Tubiello, F. N., Van Der Laan-Luijkx, I. T., Van Der Werf, G. R., Van Heuven, S., Viovy, N., Vuichard, N., Walker, A. P., Watson, A. J., Wiltshire, A. J., Zaehle, S., and Zhu, D.: Global Carbon Budget 2017, Earth Syst. Sci. Data, 10, 405–448, https://doi.org/10.5194/essd-10-405-2018, 2018.

Laurent, O., 2016. ICOS Atmospheric Station Specifications.

Lin, X., Indira, N. K., Ramonet, M., Delmotte, M., Ciais, P., Bhatt, B. C., Reddy, M. V., Angchuk, D., Balakrishnan, S., Jorphail, S., Dorjai, T., Mahey, T. T., Patnaik, S., Begum, M., Brenninkmeijer, C., Durairaj, S., Kirubagaran, R., Schmidt, M., Swathi, P. S., Vinithkumar, N. V., Yver Kwok, C., and Gaur, V. K.: Long-lived atmospheric trace gases measurements in flask samples from three stations in India, Atmos. Chem. Phys., 15, 9819–9849, https://doi.org/10.5194/acp-15-9819-2015, 2015.

Lin, X., Ciais, P., Bousquet, P., Ramonet, M., Yin, Y., Balkanski, Y., Cozic, A., Delmotte, M., Evangeliou, N., Indira, N. K., Locatelli, R., Peng, S., Piao, S., Saunois, M., Swathi, P. S., Wang, R., Yver-Kwok, C., Tiwari, Y. K., and Zhou, L.: Simulating CH_4 and CO_2 over South and East Asia using the zoomed chemistry transport model LMDz-INCA, Atmos. Chem. Phys., 18, 9475–9497, https://doi.org/10.5194/acp-18-9475-2018, 2018.

Liu, J., Bowman, K. W., Lee, M., Henze, D. K., Bousserez, N., Brix, H., Collatz, G. J., Menemenlis, D., Ott, L., Pawson, S., Jones, D., and Nassar, R.: Carbon monitoring system flux estimation and attribution: impact of ACOS-GOSAT XCO_2 sampling on the inference of terrestrial biospheric sources and sinks, Tellus B: Chemical and Physical Meteorology, 66, 22486, https://doi.org/10.3402/tellusb.v66.22486, 2014.

Lopez, M.: Estimation des émissions de gaz à effet de serre à différentes échelles en France à l'aide d'observations de haute précision, phdthesis, Université Paris Sud - Paris XI, 2012.

Mahesh, P., Sreenivas, G., Rao, P. V. N., Dadhwal, V. K., Sai Krishna, S. V. S., and Mallikarjun, K.: High-precision surface-level CO2 and CH4 using off-axis integrated cavity output spectroscopy (OA-ICOS) over Shadnagar, India, International Journal of Remote Sensing, 36, 5754–5765, https://doi.org/10.1080/01431161.2015.1104744, 2015.

Masarie, K. A., Peters, W., Jacobson, A. R., and Tans, P. P.: ObsPack: a framework for the preparation, delivery, and attribution of atmospheric greenhouse gas measurements, Earth Syst. Sci. Data, 6, 375–384, https://doi.org/10.5194/essd-6-375-2014, 2014.

Matsueda, H., Inoue, H. Y., Ishii, M., and Tsutsumi, Y.: Large injection of carbon monoxide into the upper troposphere due to intense biomass burning in 1997, J. Geophys. Res., 104, 26867–26879, https://doi.org/10.1029/1999JD900193, 1999.

Mauzerall, D. L., Logan, J. A., Jacob, D. J., Anderson, B. E., Blake, D. R., Bradshaw, J. D., Heikes, B., Sachse, G. W., Singh, H., and Talbot, B.: Photochemistry in biomass burning plumes and implications for tropospheric ozone over the tropical South Atlantic, J. Geophys. Res., 103, 8401–8423, https://doi.org/10.1029/97JD02612, 1998.

Metya, A., Datye, A., Chakraborty, S., Tiwari, Y. K., Sarma, D., Bora, A., and Gogoi, N.: Diurnal and seasonal variability of CO2 and CH4 concentration in a semi-urban environment of western India, Sci Rep, 11, 2931, https://doi.org/10.1038/s41598-021-82321-1, 2021.

Mühle, J., Brenninkmeijer, C. a. M., Rhee, T. S., Slemr, F., Oram, D. E., Penkett, S. A., and Zahn, A.: Biomass burning and fossil fuel signatures in the upper troposphere observed during a CARIBIC flight from Namibia to Germany, Geophysical Research Letters, 29, 16-1-16–4, https://doi.org/10.1029/2002GL015764, 2002.

Nalini, K., Sijikumar, S., Valsala, V., Tiwari, Y. K., and Ramachandran, R.: Designing surface CO2 monitoring network to constrain the Indian land fluxes, Atmospheric Environment, 218, 117003, https://doi.org/10.1016/j.atmosenv.2019.117003, 2019.

Nath, B.: Quantitative Assessment of Forest Cover Change of a Part of Bandarban Hill Tracts Using NDVI Techniques, Journal of Geosciences and Geomatics, 2, 21–27, https://doi.org/10.12691/jgg-2-1-4, 2014.

Nishanth, T., Praseed, K. M., Kumar, M. K. S., and Valsaraj, K. T.: Observational Study of Surface O3, NOx, CH4 and Total NMHCs at Kannur, India, Aerosol Air Qual. Res., 14, 1074–1088, https://doi.org/10.4209/aaqr.2012.11.0323, 2014.

Niwa, Y., Machida, T., Sawa, Y., Matsueda, H., Schuck, T. J., Brenninkmeijer, C. A. M., Imasu, R., and Satoh, M.: Imposing strong constraints on tropical terrestrial CO2 fluxes using passenger aircraft based measurements, Journal of Geophysical Research: Atmospheres, 117, https://doi.org/10.1029/2012JD017474, 2012.

Nomura, S., Naja, M., Ahmed, M. K., Mukai, H., Terao, Y., Machida, T., Sasakawa, M., and Patra, P. K.: Measurement report: Regional characteristics of seasonal and long-term variations in greenhouse gases at Nainital, India, and Comilla, Bangladesh, Atmos. Chem. Phys., 21, 16427–16452, https://doi.org/10.5194/acp-21-16427-2021, 2021.

Ott, L. E., Pawson, S., Collatz, G. J., Gregg, W. W., Menemenlis, D., Brix, H., Rousseaux, C. S., Bowman, K. W., Liu, J., Eldering, A., Gunson, M. R., and Kawa, S. R.: Assessing the magnitude of CO_2 flux uncertainty in atmospheric CO_2 records using products from NASA's Carbon Monitoring Flux Pilot Project, JGR Atmospheres, 120, 734–765, https://doi.org/10.1002/2014JD022411, 2015.

Paris, J.-D., Ciais, P., Nédélec, P., Ramonet, M., Belan, B. D., Arshinov, M. Yu., Golitsyn, G. S., Granberg, I., Stohl, A., Cayez, G., Athier, G., Boumard, F., and Cousin, J.-M.: The YAK-AEROSIB transcontinental aircraft campaigns: new insights on the transport of CO2, CO and O3 across Siberia, Tellus B: Chemical and Physical Meteorology, 60, 551–568, https://doi.org/10.1111/j.1600-0889.2008.00369.x, 2008.

Park, M., Randel, W. J., Emmons, L. K., and Livesey, N. J.: Transport pathways of carbon monoxide in the Asian summer monsoon diagnosed from Model of Ozone and Related Tracers (MOZART), J. Geophys. Res., 114, 2008JD010621, https://doi.org/10.1029/2008JD010621, 2009.

Pathakoti, M., D.V., M., Gaddamidi, S., Arun, S. S., Bothale, R. V., Chauhan, P., P, R., K.S., R., and Chandra, N.: Three-dimensional view of CO2 variability in the atmosphere over the

https://doi.org/10.5194/egusphere-2025-3538
Preprint. Discussion started: 29 September 2025

Indian region, Atmospheric Research, 290, 106785, https://doi.org/10.1016/j.atmosres.2023.106785, 2023.

Patil, M. N., Dharmaraj, T., Waghmare, R. T., Prabha, T. V., and Kulkarni, J. R.: Measurements of carbon dioxide and heat fluxes during monsoon-2011 season over rural site of India by eddy covariance technique, J Earth Syst Sci, 123, 177–185, https://doi.org/10.1007/s12040-013-0374-z, 2014.

Patra, P. K., Niwa, Y., Schuck, T. J., Brenninkmeijer, C. a. M., Machida, T., Matsueda, H., and Sawa, Y.: Carbon balance of South Asia constrained by passenger aircraft CO_2 measurements, Atmospheric Chemistry and Physics, 11, 4163–4175, https://doi.org/10.5194/acp-11-4163-2011, 2011.

Patra, P. K., Canadell, J. G., Houghton, R. A., Piao, S. L., Oh, N.-H., Ciais, P., Manjunath, K. R., Chhabra, A., Wang, T., Bhattacharya, T., Bousquet, P., Hartman, J., Ito, A., Mayorga, E., Niwa, Y., Raymond, P. A., Sarma, V. V. S. S., and Lasco, R.: The carbon budget of South Asia, Biogeosciences, 10, 513–527, https://doi.org/10.5194/bg-10-513-2013, 2013.

Patra, P. K., Crisp, D., Kaiser, J. W., Wunch, D., Saeki, T., Ichii, K., Sekiya, T., Wennberg, P. O., Feist, D. G., Pollard, D. F., Griffith, D. W. T., Velazco, V. A., De Maziere, M., Sha, M. K., Roehl, C., Chatterjee, A., and Ishijima, K.: The Orbiting Carbon Observatory (OCO-2) tracks 2–3 peta-gram increase in carbon release to the atmosphere during the 2014–2016 El Niño, Sci Rep, 7, 13567, https://doi.org/10.1038/s41598-017-13459-0, 2017.

Patra, P. K., Takigawa, M., Watanabe, S., Chandra, N., Ishijima, K., and Yamashita, Y.: Improved Chemical Tracer Simulation by MIROC4.0-based Atmospheric Chemistry-Transport Model (MIROC4-ACTM), Sola, 14, 91–96, https://doi.org/10.2151/sola.2018-016, 2018.

Peters, W., Miller, J. B., Whitaker, J., Denning, A. S., Hirsch, A., Krol, M. C., Zupanski, D., Bruhwiler, L., and Tans, P. P.: An ensemble data assimilation system to estimate CO2 surface fluxes from atmospheric trace gas observations, Journal of Geophysical Research: Atmospheres, 110, https://doi.org/10.1029/2005JD006157, 2005.

Philip, S., Johnson, M. S., Potter, C., Genovesse, V., Baker, D. F., Haynes, K. D., Henze, D. K., Liu, J., and Poulter, B.: Prior biosphere model impact on global terrestrial CO_2 fluxes estimated from OCO-2 retrievals, Atmos. Chem. Phys., 19, 13267–13287, https://doi.org/10.5194/acp-19-13267-2019, 2019.

Philip, S., Johnson, M. S., Baker, D. F., Basu, S., Tiwari, Y. K., Indira, N. K., Ramonet, M., and Poulter, B.: OCO-2 Satellite-Imposed Constraints on Terrestrial Biospheric CO_2 Fluxes Over South Asia, JGR Atmospheres, 127, e2021JD035035, https://doi.org/10.1029/2021JD035035, 2022.

Potter, C. S., Randerson, J. T., Field, C. B., Matson, P. A., Vitousek, P. M., Mooney, H. A., and Klooster, S. A.: Terrestrial ecosystem production: A process model based on global satellite and surface data, Global Biogeochemical Cycles, 7, 811–841, https://doi.org/10.1029/93GB02725, 1993.

Randel, W. J. and Park, M.: Deep convective influence on the Asian summer monsoon anticyclone and associated tracer variability observed with Atmospheric Infrared Sounder

https://doi.org/10.5194/egusphere-2025-3538
Preprint. Discussion started: 29 September 2025

(AIRS), Journal of Geophysical Research: Atmospheres, 111, https://doi.org/10.1029/2005JD006490, 2006.

Randerson, J. T., Thompson, M. V., Conway, T. J., Fung, I. Y., and Field, C. B.: The contribution of terrestrial sources and sinks to trends in the seasonal cycle of atmospheric carbon dioxide, Global Biogeochemical Cycles, 11, 535–560, https://doi.org/10.1029/97GB02268, 1997.

Rathore, J., Ganguly, D., Singh, V., Gupta, M., Vazhathara, V. J., Biswal, A., Kunchala, R. K., Patra, P. K., Sahu, L. K., Gani, S., and Dey, S.: Characteristics of Haze Pollution Events During Biomass Burning Period at an Upwind Site of Delhi, JGR Atmospheres, 130, e2024JD042347, https://doi.org/10.1029/2024JD042347, 2025.

Rayner, P. J., Law, R. M., Allison, C. E., Francey, R. J., Trudinger, C. M., and Pickett-Heaps, C.: Interannual variability of the global carbon cycle (1992–2005) inferred by inversion of atmospheric CO2 and δ13CO2 measurements, Global Biogeochemical Cycles, 22, https://doi.org/10.1029/2007GB003068, 2008.

Reid, K. H. and Steyn, D. G.: Diurnal variations of boundary-layer carbon dioxide in a coastal city—Observations and comparison with model results, Atmospheric Environment, 31, 3101–3114, https://doi.org/10.1016/S1352-2310(97)00050-2, 1997.

Russo, R. S., Talbot, R. W., Dibb, J. E., Scheuer, E., Seid, G., Jordan, C. E., Fuelberg, H. E., Sachse, G. W., Avery, M. A., Vay, S. A., Blake, D. R., Blake, N. J., Atlas, E., Fried, A., Sandholm, S. T., Tan, D., Singh, H. B., Snow, J., and Heikes, B. G.: Chemical composition of Asian continental outflow over the western Pacific: Results from Transport and Chemical Evolution over the Pacific (TRACE-P), Journal of Geophysical Research: Atmospheres, 108, https://doi.org/10.1029/2002JD003184, 2003.

Sawa, Y., Matsueda, H., Makino, Y., Inoue, H. Y., Murayama, S., Hirota, M., Tsutsumi, Y., Zaizen, Y., Ikegami, M., and Okada, K.: Aircraft Observation of CO_2, CO_2 O_3 and H_2 over the North Pacific during the PACE-7 Campaign, Tellus B: Chemical and Physical Meteorology, 56, 2, https://doi.org/10.3402/tellusb.v56i1.16402, 2004.

Schaaf, C. and Wang, Z.: MODIS/Terra+Aqua BRDF/Albedo Nadir BRDF-Adjusted Ref Band6 Daily L3 Global 30ArcSec CMG V061, https://doi.org/10.5067/MODIS/MCD43D67.061, 2021.

Schaaf, C. B., Gao, F., Strahler, A. H., Lucht, W., Li, X., Tsang, T., Strugnell, N. C., Zhang, X., Jin, Y., Muller, J.-P., Lewis, P., Barnsley, M., Hobson, P., Disney, M., Roberts, G., Dunderdale, M., Doll, C., d'Entremont, R. P., Hu, B., Liang, S., Privette, J. L., and Roy, D.: First operational BRDF, albedo nadir reflectance products from MODIS, Remote Sensing of Environment, 83, 135–148, https://doi.org/10.1016/S0034-4257(02)00091-3, 2002.

Schuck, T. J., Ishijima, K., Patra, P. K., Baker, A. K., Machida, T., Matsueda, H., Sawa, Y., Umezawa, T., Brenninkmeijer, C. a. M., and Lelieveld, J.: Distribution of methane in the tropical upper troposphere measured by CARIBIC and CONTRAIL aircraft, Journal of Geophysical Research: Atmospheres, 117, https://doi.org/10.1029/2012JD018199, 2012.

Schuldt, K. N., Mund, J., Aalto, T., Abshire, J. B., Aikin, K., Allen, G., Andrade, M., Arlyn Andrews, Apadula, F., Arnold, S., Baier, B., Bakwin, P., Bäni, L., Bartyzel, J., Bentz, G.,

https://doi.org/10.5194/egusphere-2025-3538
Preprint. Discussion started: 29 September 2025

Bergamaschi, P., Beyersdorf, A., Biermann, T., Biraud, S. C., Pierre-Eric Blanc, Boenisch, H., Bowling, D., Brailsford, G., Brand, W. A., Brunner, D., Bui, T. P. V., Van Den Bulk, P., Benoit Burban, Francescopiero Calzolari, Chang, C. S., Chen, G., Huilin Chen, Lukasz Chmura, St. Clair, J. M., Clark, S., Sites Climadat, Coletta, J. D., Colomb, A., Commane, R., Condori, L., Conen, F., Conil, S., Couret, C., Cristofanelli, P., Cuevas, E., Curcoll, R., Daube, B., Davis, K. J., Dean-Day, J. M., Delmotte, M., Dickerson, R., DiGangi, E., DiGangi, J. P., Van Dinther, D., Elsasser, M., Emmenegger, L., Shuangxi Fang, Forster, G., France, J., Frumau, A., Fuente-Lastra, M., Galkowski, M., Gatti, L. V., Gehrlein, T., Gerbig, C., Francois Gheusi, Gloor, E., Goto, D., Griffis, T., Hammer, S., Hanisco, T. F., Hanson, C., Haszpra, L., Hatakka, J., Heimann, M., Heliasz, M., Heltai, D., Henne, S., Hensen, A., Hermans, C., Hermansen, O., Hintsa, E., Hoheisel, A., Holst, J., Di Iorio, T., Iraci, L. T., Ivakhov, V., Jaffe, D. A., Jordan, A., Joubert, W., Kang, H.-Y., Karion, A., Kawa, S. R., Kazan, V., Keeling, R. F., Keronen, P., Jooil Kim, Klausen, J., Kneuer, T., et al.: Multi-laboratory compilation of atmospheric carbon dioxide data for the period 1957-2023; obspack_co2_1_GLOBALVIEWplus_v10.1_2024-11-13, https://doi.org/10.25925/20241101, 2024.

Sharma, N., Dadhwal, V. K., Kant, Y., Mahesh, P., Mallikarjun, K., Gadavi, H., Sharma, A., and Ali, M. M.: Atmospheric CO2 Variations in Two Contrasting Environmental Sites Over India, Air, Soil and Water Research, 7, ASWR.S13987, https://doi.org/10.4137/ASWR.S13987, 2014.

Singh, A., Abbhishek, K., Kuttippurath, J., Raj, S., Mallick, N., Chander, G., and Dixit, S.: Decadal variations in CO2 during agricultural seasons in India and role of management as sustainable approach, Environmental Technology & Innovation, 27, 102498, https://doi.org/10.1016/j.eti.2022.102498, 2022.

Sreenivas, G., Mahesh, P., Subin, J., Kanchana, A. L., Rao, P. V. N., and Dadhwal, V. K.: Influence of Meteorology and interrelationship with greenhouse gases (CO₂ and CH₄) at a suburban site of India, Atmos. Chem. Phys., 16, 3953–3967, https://doi.org/10.5194/acp-16-3953-2016, 2016.

Sreenivas, G., P., M., Mahalakshmi, D. V., Kanchana, A. L., Chandra, N., Patra, P. K., Raja, P., Sesha Sai, M. V. R., Sripada, S., Rao, P. V. N., and Dadhwal, V. K.: Seasonal and annual variations of CO2 and CH4 at Shadnagar, a semi-urban site, Science of The Total Environment, 819, 153114, https://doi.org/10.1016/j.scitotenv.2022.153114, 2022.

Srivastava, P., Bennett, M. W., Bedrosian, G., Rosenberg, R., Solish, B., and Basilio, R. R.: Establishing Launch Readiness of NASA ISS Instrument OCO-3, in: IGARSS 2020 - 2020 IEEE International Geoscience and Remote Sensing Symposium, IGARSS 2020 - 2020 IEEE International Geoscience and Remote Sensing Symposium, Waikoloa, HI, USA, 6101–6104, https://doi.org/10.1109/IGARSS39084.2020.9323631, 2020.

Stocker, T.F., D. Qin, G.-K. Plattner, L.V. Alexander, S.K. Allen, N.L. Bindoff, F.-M. Bréon, J.A. Church, U. Cubasch, S. Emori, P. Forster, P. Friedlingstein, N. Gillett, J.M. Gregory, D.L. Hartmann, E. Jansen, B. Kirtman, R. Knutti, K. Krishna Kumar, P. Lemke, J. Marotzke, V.Masson-Delmotte, G.A. Meehl, I.I. Mokhov, S. Piao, V. Ramaswamy, D. Randall, M. Rhein,M. Rojas, C. Sabine, D. Shindell, L.D. Talley, D.G. Vaughan and S.-P. Xie, 2013: Technical Summary. In: Climate Change 2013: The Physical Science Basis. Contribution of Working Group I to the Fifth Assessment Report of the Intergovernmental Panel on Climate Change [Stocker, T.F., D. Qin, G.-K. Plattner, M. Tignor, S.K. Allen, J. Boschung, A.

https://doi.org/10.5194/egusphere-2025-3538
Preprint. Discussion started: 29 September 2025

Nauels, Y. Xia, V. Bex and P.M. Midgley (eds.)]. Cambridge University Press, Cambridge, United Kingdom and New York, NY, USA

Stull, R. B. (Ed.): An Introduction to Boundary Layer Meteorology, Springer Netherlands, Dordrecht, https://doi.org/10.1007/978-94-009-3027-8, 1988.

Summa, D., Di Girolamo, P., Stelitano, D., and Cacciani, M.: Characterization of the planetary boundary layer height and structure by Raman lidar: comparison of different approaches, Atmospheric Measurement Techniques, 6, 3515–3525, https://doi.org/10.5194/amt-6-3515-2013, 2013.

Sun, Y., Frankenberg, C., Jung, M., Joiner, J., Guanter, L., Köhler, P., and Magney, T.: Overview of Solar-Induced chlorophyll Fluorescence (SIF) from the Orbiting Carbon Observatory-2: Retrieval, cross-mission comparison, and global monitoring for GPP, Remote Sensing of Environment, 209, 808–823, https://doi.org/10.1016/j.rse.2018.02.016, 2018.

Thilakan, V., Pillai, D., Sukumaran, J., Gerbig, C., Hakkim, H., Sinha, V., Terao, Y., Naja, M., and Deshpande, M. V.: Potential of using CO_2 observations over India in regional carbon budget estimation by improving the modelling system, EGUsphere, 1–32, https://doi.org/10.5194/egusphere-2023-1582, 2023.

Tiwari, Y., Valsala, V., Vellore, R., and Kunchala, R.: Effectiveness of surface monitoring stations in representing regional CO<sub>2 emissions over India, Clim. Res., 56, 121–129, https://doi.org/10.3354/cr01149, 2013.

Tiwari, Y. K., Vellore, R. K., Ravi Kumar, K., Van Der Schoot, M., and Cho, C.-H.: Influence of monsoons on atmospheric CO2 spatial variability and ground-based monitoring over India, Science of The Total Environment, 490, 570–578, https://doi.org/10.1016/j.scitotenv.2014.05.045, 2014.

Vermote, E. and NOAA CDR Program: NOAA Climate Data Record (CDR) of AVHRR Normalized Difference Vegetation Index (NDVI), Version 5, https://doi.org/10.7289/V5ZG6QH9, 2018.

Wada, A., Matsueda, H., Sawa, Y., Tsuboi, K., and Okubo, S.: Seasonal variation of enhancement ratios of trace gases observed over 10 years in the western North Pacific, Atmospheric Environment, 45, 2129–2137, https://doi.org/10.1016/j.atmosenv.2011.01.043, 2011.

Wang, G., Huang, J., Guo, W., Zuo, J., Wang, J., Bi, J., Huang, Z., and Shi, J.: Observation analysis of land-atmosphere interactions over the Loess Plateau of northwest China, Journal of Geophysical Research: Atmospheres, 115, https://doi.org/10.1029/2009JD013372, 2010.

Wang, Z., Schaaf, C. B., Sun, Q., Shuai, Y., and Román, M. O.: Capturing rapid land surface dynamics with Collection V006 MODIS BRDF/NBAR/Albedo (MCD43) products, Remote Sensing of Environment, 207, 50–64, https://doi.org/10.1016/j.rse.2018.02.001, 2018.

Watanabe, S., Miura, H., Sekiguchi, M., Nagashima, T., Sudo, K., Emori, S., and Kawamiya, M.: Development of an atmospheric general circulation model for integrated Earth system modeling on the Earth Simulator, Earth Simulator, 9, 27–35, 2008.

https://doi.org/10.5194/egusphere-2025-3538
Preprint. Discussion started: 29 September 2025

Weir, B., Ott, L. E., Collatz, G. J., Kawa, S. R., Poulter, B., Chatterjee, A., Oda, T., and Pawson, S.: Bias-correcting carbon fluxes derived from land-surface satellite data for retrospective and near-real-time assimilation systems, Atmos. Chem. Phys., 21, 9609–9628, https://doi.org/10.5194/acp-21-9609-2021, 2021a.

Weir, B., Crisp, D., O'Dell, C. W., Basu, S., Chatterjee, A., Kolassa, J., Oda, T., Pawson, S., Poulter, B., Zhang, Z., Ciais, P., Davis, S. J., Liu, Z., and Ott, L. E.: Regional impacts of COVID-19 on carbon dioxide detected worldwide from space, Sci. Adv., 7, eabf9415, https://doi.org/10.1126/sciadv.abf9415, 2021b.

Worthy, D. E. J., Chan, E., Ishizawa, M., Chan, D., Poss, C., Dlugokencky, E. J., Maksyutov, S., and Levin, I.: Decreasing anthropogenic methane emissions in Europe and Siberia inferred from continuous carbon dioxide and methane observations at Alert, Canada, Journal of Geophysical Research: Atmospheres, 114, https://doi.org/10.1029/2008JD011239, 2009.

Xiao, Y., Jacob, D. J., Wang, J. S., Logan, J. A., Palmer, P. I., Suntharalingam, P., Yantosca, R. M., Sachse, G. W., Blake, D. R., and Streets, D. G.: Constraints on Asian and European sources of methane from CH_4 -C_2 H_6 -CO correlations in Asian outflow, J. Geophys. Res., 109, 2003JD004475, https://doi.org/10.1029/2003JD004475, 2004.

Xiong, X., Houweling, S., Wei, J., Maddy, E., Sun, F., and Barnet, C.: Methane plume over south Asia during the monsoon season: satellite observation and model simulation, Atmospheric Chemistry and Physics, 9, 783–794, https://doi.org/10.5194/acp-9-783-2009, 2009.

Yoro, K. O. and Daramola, M. O.: CO2 emission sources, greenhouse gases, and the global warming effect, in: Advances in Carbon Capture, Elsevier, 3–28, https://doi.org/10.1016/B978-0-12-819657-1.00001-3, 2020.

Yuan, Y., Ries, L., Petermeier, H., Steinbacher, M., Gómez-Peláez, A. J., Leuenberger, M. C., Schumacher, M., Trickl, T., Couret, C., Meinhardt, F., and Menzel, A.: Adaptive selection of diurnal minimum variation: a statistical strategy to obtain representative atmospheric CO_2 data and its application to European elevated mountain stations, Atmospheric Measurement Techniques, 11, 1501–1514, https://doi.org/10.5194/amt-11-1501-2018, 2018.

Zhang, H. F., Chen, B. Z., van der Laan-Luijk, I. T., Machida, T., Matsueda, H., Sawa, Y., Fukuyama, Y., Langenfelds, R., van der Schoot, M., Xu, G., Yan, J. W., Cheng, M. L., Zhou, L. X., Tans, P. P., and Peters, W.: Estimating Asian terrestrial carbon fluxes from CONTRAIL aircraft and surface CO_2 observations for the period 2006–2010, Atmospheric Chemistry and Physics, 14, 5807–5824, https://doi.org/10.5194/acp-14-5807-2014, 2014.

Zhang, X., Nakazawa, T., Ishizawa, M., Aoki, S., Nakaoka, S.-I., Sugawara, S., Maksyutov, S., Saeki, T., and Hayasaka, T.: Temporal variations of atmospheric carbon dioxide in the southernmost part of Japan, Tellus B: Chemical and Physical Meteorology, 59, 654–663, https://doi.org/10.1111/j.1600-0889.2007.00288.x, 2007.